Cuadernos de Investigación Geográfica *Geographical Research Letters*	2026	Nº 52	pp. xx-xx	EISSN 1697-9540

http://doi.org/10.18172/cig.6683

INTEGRATION OF MACHINE LEARNING MODELS AND SPATIAL SIMULATION FOR LAND USE CHANGE ANALYSIS IN LOJA, ECUADOR

IVONNE GONZÁLEZ-CORONEL[1]*, VERÓNICA MUÑOZ-SOTOMAYOR[2], MARÍA FERNANDA BURNEO-ORDÓÑEZ[1]

[1]*Departamento de Ciencias Biológicas y Agropecuarias, Facultad de Ciencias Exactas y Naturales, Universidad Técnica Particular de Loja UTPL, Loja, Ecuador.*

[2]*Universidad Internacional del Ecuador UIDE, Loja, Ecuador.*

ABSTRACT. This study analyzed land-use change patterns in Loja, Ecuador, between 1990 and 2020 using transition matrices and the change intensity methodological framework. Based on these spatiotemporal dynamics, urban expansion was projected to 2070, and alternative scenarios were generated. To explain current dynamics, the Random Forest model achieved the best performance (accuracy: 90.72%; Kappa: 0.852; quantity disagreement: 0.04; allocation disagreement: 0.17). In the trend scenario for 2070, urban expansion would primarily affect agricultural areas (93.6%) and natural vegetation (6.15%), including approximately 17.2% of zones with a high landslide risk. Under future climate scenarios, this expansion is expected to be concentrated in areas with projected increases in temperature and precipitation, potentially heightening the city's vulnerability to extreme events. The results highlight the usefulness of open-access tools for modeling future urban scenarios in data-limited contexts, as well as the replicability of the methodology in other intermediate cities facing similar challenges. Overall, this study contributes to the design of sustainable land management strategies tailored to local contexts.

Integración de modelos de aprendizaje automático y simulación espacial para el análisis del cambio de uso del suelo en Loja, Ecuador

RESUMEN. Este estudio analizó los patrones de cambio de uso del suelo en Loja, Ecuador, entre 1990 y 2020 mediante matrices de transición y el marco metodológico de la intensidad de cambio. A partir de estas dinámicas espacio-temporales, se proyectó la expansión urbana hasta 2070 y se generaron escenarios alternativos. Para explicar las dinámicas actuales, el modelo Random Forest presentó el mejor desempeño (precisión: 90,72 %; Kappa: 0,852; desacuerdo en cantidad: 0,04; desacuerdo en ubicación: 0,17). En el escenario tendencial para 2070, la expansión urbana afectaría principalmente áreas agrícolas (93,6 %) y la vegetación natural (6,15 %), incluyendo aproximadamente el 17,2 % de las zonas de alto riesgo de deslizamientos. En escenarios climáticos futuros, esta expansión se concentraría en áreas con incrementos proyectados de temperatura y precipitación, lo que podría aumentar la vulnerabilidad a eventos extremos. Los resultados evidencian la utilidad de herramientas de acceso libre para modelar escenarios urbanos futuros en contextos con limitaciones de datos, así como la replicabilidad de la metodología en otras ciudades intermedias con desafíos similares, lo que contribuye al diseño de estrategias sostenibles de gestión territorial adaptadas a contextos locales.

Key words: Land use changes, machine learning models, Ecuador.

Palabras clave: cambios de uso del suelo, modelos de aprendizaje automático, Ecuador.

Received: 1 April 2025

Accepted: 1 October 2025

***Corresponding author:** Ivonne González-Coronel, Departamento de Ciencias Biológicas y Agropecuarias, Facultad de Ciencias Exactas y Naturales, Universidad Técnica Particular de Loja UTPL, Loja, Ecuador. Email: imgonzalez3@utpl.edu.ec

1. Introduction

Urban expansion is a global phenomenon characterized by region-specific patterns. In Latin America, many cities are classified as mid-sized (Wu *et al.,* 2021), and their growth is driven by population increases, economic transformations, migration, and the conversion of rural land to urban use (Mahtta *et al.,* 2022). This growth pattern brings negative impacts, including uncontrolled land consumption, rising carbon emissions, and the loss of natural habitats (Lu et *al.,* 2023; Mou *et al*., 2023; Ouma *et al.,* 2024).

To address these challenges, several studies underscore the critical role of land-use change simulation models. These models not only anticipate future scenarios but also provide insights for designing strategies. Such strategies help foster sustainable ecosystem management and mitigate environmental degradation. They also support efforts aligned with SDGs 11 (Sustainable Cities) and 15 (Life on Land) (Mou *et al.,* 2023; Ouma *et al.,* 2024; Tahir *et al.,* 2025).

Over recent decades, land use change modeling has advanced considerably due to the availability of open spatial data from global initiatives such as MapBiomas (Souza *et al.,* 2020), open-source tools like the MOLUSCE plugin for QGIS, the Land Change Modeler module in Terrset (Leta *et al.,* 2021; Lukas *et al.,* 2023), and cloud-based platforms such as Google Earth Engine (Faheem *et al.,* 2024). These resources support the implementation of both traditional statistical techniques, such as Logistic Regression (LR), and more advanced machine learning approaches, such as Artificial Neural Networks (ANN) and Random Forest (RF) (Hagenauer *et al.,* 2019; Nong and Du, 2011; Sankarrao *et al.*, 2021). Among statistical models, LR is widely used due to its simplicity but faces limitations in contexts with nonlinear relationships or spatial autocorrelation (Alsharif and Pradhan, 2013; Lin *et al.,* 2010; Mei and Li, 2018; Pradana *et al.,* 2023). In contrast, ANN and RF can better represent complex urban dynamics, particularly in areas with irregular topography (Hagenauer *et al.,* 2019; Zhu *et al.,* 2024). ANN achieves high accuracy but is challenging to interpret (Kafy *et al.,* 2020; Lukas *et al.,* 2023), while RF minimizes overfitting and performs well in urban environments (Faheem *et al.,* 2024; Mutale *et al.,* 2024). However, the choice of model depends on the study context and data availability (Hagenauer *et al.,* 2019).

Developing accurate and reliable land-use change models begins by identifying and representing the main drivers of such change (Veldkamp and Lambin, 2001). These include biophysical factors such as topography, climate, water bodies, and lithology, as well as socioeconomic variables like population density, migration, employment, and access to services, all of which influence residential location decisions (Gallardo, 2018). It is also essential to simulate the decisions of multiple actors involved in land management, as well as public policies and land-use regulations, since these dynamics directly shape landscape transformation (Malek *et al.,* 2019). This highlights the complexity of predicting land use changes. Additionally, methods such as intensity analysis (Aldwaik and Pontius, 2012; Pontius *et al.*, 2004) offer critical insights into current patterns and into projecting future scenarios (Deng and Quan, 2022).

Within this context, this study analyzes urban expansion in Loja, Ecuador. This inter-Andean city has experienced an 82% increase in urban area, outpacing population growth and ranking among Ecuador's most rapidly expanding intermediate cities in recent decades (MIDUVI, 2015). The city's geomorphological characteristics and steep terrain make it highly vulnerable to climate change (FIC *et al.,* 2021). However, local planning instruments do not incorporate methodologies that use simulation models to improve land management efficiency. Moreover, urban development has historically been

allowed in areas designated as non-developable under current plans (Municipio de Loja, 2021). Applying simulation models in this context allows for the evaluation of future urban growth under climate change and provides practical insights for sustainable land management.

This study examines land-use and land-cover (LULC) change patterns in Loja between 1990 and 2020. The specific objectives are: (1) to analyze spatial and temporal trends of LULC across different periods between 1990 and 2020, characterizing change intensity; (2) to compare the performance of statistical and machine learning models in generating plausible land use change scenarios through 2070; and (3) to assess the implications of urban growth in areas of risk, fragile ecosystems, and productive land, under current and future climate conditions.

2. Study area

The city of Loja is located in the Cuxibamba Valley in southern Ecuador's inter-Andean region (Fig. 1). It lies at an average elevation of 2,100 m above sea level, covers an area of 57.33 km², and has an estimated population of 250,770. The city has a temperate climate, with an annual average temperature of 18 °C and precipitation of 700-800 mm (PNUMA *et al.,* 2007). This rainfall pattern, typical of a semi-humid mesothermal climate, increases the city's exposure to climate-related hazards such as landslides and floods (Municipio de Loja, 2021).

Loja's urban morphology is shaped by its elevation range, which varies from 1,880 to 3,438 meters above sea level, creating steep slopes to the east and west. These topographic constraints, along with unfavorable geological conditions for construction, limit urban growth. Human pressure on land and socioeconomic inequalities have intensified the city's vulnerability to climate change, particularly in the western area, where informal settlements and marginalized neighborhoods face recurrent threats, including landslides caused by surface and subsurface runoff and prolonged droughts (FIC *et al.,* 2021).

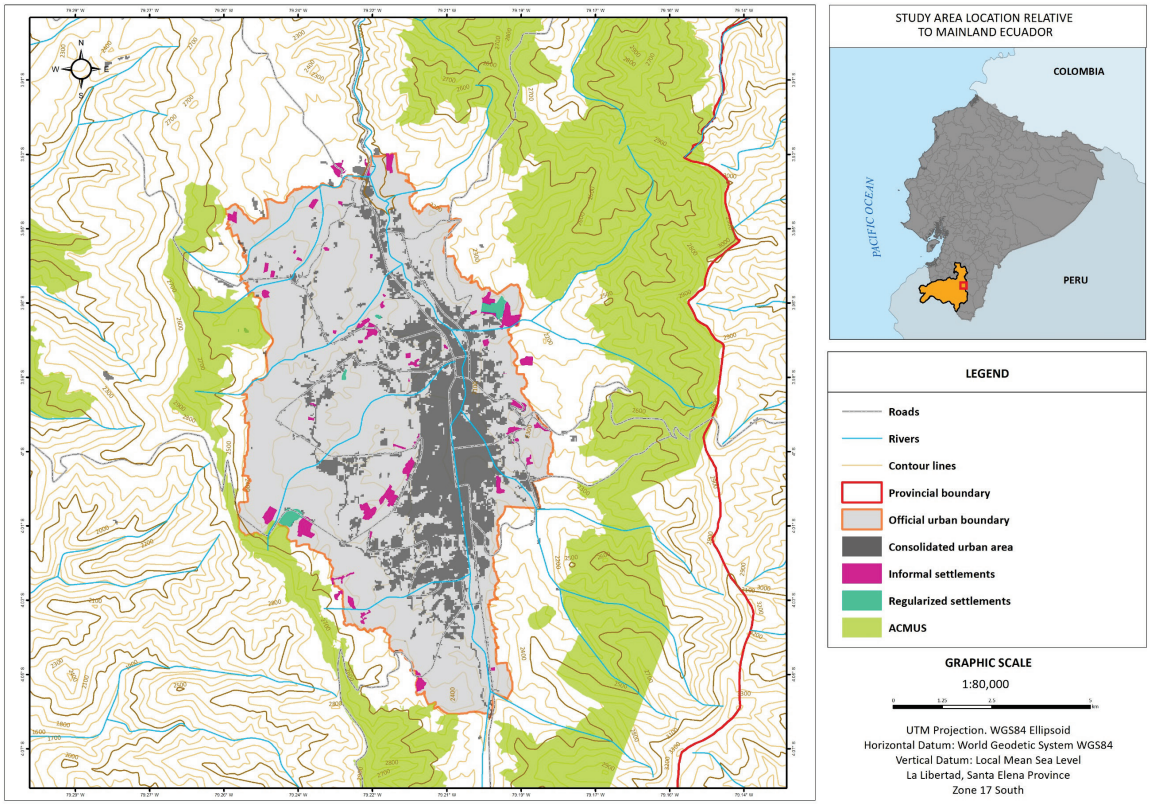

Figure 1. Location map of the city of Loja.

Between 2010 and 2022, 956 hazardous events were reported within the urban perimeter, affecting over 5,000 people and 1,000 houses, mainly due to human causes and rainfall-related events (Gobierno de Ecuador, 2024a; SNGR, 2025). In recent years, these events have increased in frequency and impact, making Loja province the third-most-affected province in Ecuador by climate-related events between 2010 and 2024 (Gobierno de Ecuador, 2024b).

Population growth, migration, and real estate pressure have transformed the urban landscape, particularly affecting fragile ecosystems, water sources, and protected areas. In response, about 10,000 ha were designated in 2020 as Municipal Conservation and Sustainable Use Areas (Áreas de Conservación y Uso Sostenible, ACMUS) through a municipal ordinance intended to regulate environmental functions (Municipio de Loja, 2020). Nevertheless, urban expansion continues to threaten these zones due to weak planning frameworks. The combination of environmental conditions, high climate vulnerability, morphological constraints, and planning deficiencies makes Loja a relevant case study for simulating future urban scenarios and examining the impacts of ongoing urban growth trends.

3. Materials and methods

3.1. Data preparation

We modeled land-use change in Loja using 1990, 2000, 2010, and 2020 land-cover maps from MapBiomas Ecuador, based on 30-meter Landsat imagery (MapBiomas, 2025). To ensure consistency, we reclassified the original map classes into five main categories: forest, water, agricultural land, other natural vegetation, and anthropogenic areas (see supplementary material A).

A wide set of explanatory variables was explored, combining a literature review with a detailed analysis of local conditions. Pairwise correlations among continuous variables were evaluated using Pearson's coefficient, where $|r| > 0.8$ indicated high collinearity (Ortega-Andrade *et al.,* 2021; Gündüz, 2025). In such cases, only the variable with greater conceptual relevance and data availability was retained. Subsequently, Cramer's V index was computed to measure the strength of association between each explanatory variable and the transition to anthropogenic use. Only variables with Cramer's $V > 0.15$ were included in the modeling, following previous studies (Silva *et al.,* 2019).

After applying these filters, the selected variables included both biophysical and socioeconomic factors such as elevation, slope, hydrographic network, vegetation greenness, road network, urban facilities, migration, and population density (Allan *et al.,* 2022; Alshari and Gawali, 2022; Bell *et al.,* 2010; Gao *et al.,* 2023; Kafy *et al.,* 2020; Muhammad *et al.,* 2022; Zhang *et al.,* 2021) (Table 1). For the Landsat data, all variables were standardized with respect to geographic projection, pixel size (30 m), and data format. Vector layers (shapefiles) were rasterized and converted into distance variables (e.g., distance to rivers, roads, and urban facilities).

Table 1. Variables selected for modeling land cover and land use change.

Variable	Description	Year	Source
Elevation	Pixel elevation (Digital Elevation Model – SRTM V4 – GEE).	2008	SRTM – GEE
Slope	Pixel slope in degrees derived from the DEM (SRTM V4 – GEE).	2008	SRTM – GEE
Hydrographic network	Euclidean distance from the pixel to rivers and streams.	2003	PROMSA

Vegetation greenness	Computed from Landsat 4–5 TM Collection 2 Level-2. The Normalized Difference Vegetation Index (NDVI) was calculated as the difference between the near-infrared (NIR) and red bands, serving as a proxy for vegetation greenness.	2000	https://earthexplorer.usgs.gov/
Road network	Euclidean distance from the pixel to main roads.	2003	http://geoportal.agricultura.gob.ec/index.php
Migration	Number of migrants per census sector.	2001	National Census 2001 (https://www.ecuadorencifras.gob.ec/estadisticas/)
Urban facilities	Euclidean distance from the pixel to the nearest focal point within the city (commercial, administrative, health, or educational sites).	2010	http://www.sigtierras.gob.ec/fotografia-aerea-y-ortofotos/

3.2. Land Use Change Analysis

To analyze land use changes, we generated transition matrices for 1990-2000, 2000-2010, and 2010-2020. Using these matrices, we calculated change indicators as described in Pontius *et al.* (2004), measuring persistence, losses, gains, swaps, total change, and net change in land use categories. We then assessed change dynamics at three hierarchical levels—interval, category, and transition—as specified by Aldwaik and Pontius (2012) (Table 2).

Table 2. Equations for calculating change intensity.

Level	Indicator	Equation
Interval	Annual change intensity (S_t)	$S_t = ((C / d) / A) * 100$
	Uniform intensity (U)	$U = (((\Sigma C_t) / D\_total) / A) * 100$
Category	Gain intensity of category *j* (G_{tj})	$G_{tj} = ((g_j / d) / c_j) * 100$
	Loss intensity of category *i* (L_{ti})	$L_{ti} = ((l_i / d) / r_i) * 100$
Transition	Observed transition intensity $i \rightarrow n$ (R_{tin})	$R_{tin} = ((M_{in} / d) / r_i) * 100$
	Expected uniform intensity for gaining category *n* (W_{tn})	$W_{tn} = ((g_n / d) / (A - r_n)) * 100$

Note: A = total study area; d = duration of the interval (years); C = total change (area that changed category); C_t = total change in interval t; D_total = total study duration; g_j = gross gain of category *j*; l_i = gross loss of category *i*; c_j = area of category *j* in Y_{t+1}; r_i = area of category *i* in Y_t; M_{in} = area that was *i* in Y_t and became *n* in Y_{t+1}; r_n = area of category *n* in Y_t.

3.3. Land Use Change Modelling

To further investigate land-use change, we applied simulation models to synthesize complex urban dynamics in an interpretable manner (Muhammad *et al.,* 2022). Three modeling approaches—Random Forest (RF), Artificial Neural Networks (ANN), and Logistic Regression (LR)—were used to estimate transition potentials and simulate future land use changes. The models were trained using transition data from 2000 to 2010 and the selected explanatory variables.

The Random Forest model used the Land Change Modeler in TerrSet liberaGIS (Varnier and Webber, 2025) with a sample size of 5 per class, two variables per split, and 100 trees. The ANN and LR models were run in QGIS using the MOLUSCE plugin (https://nextgis.com/molusce/) (Kamaraj and Rangarajan, 2022). The ANN had 5,000 iterations, a 2 × 2-pixel neighborhood, six hidden layers, a learning rate of 0.05, and a momentum of 0.04. The LR model used 5,000 iterations and a Moore 5 × 5-cell neighborhood (Samat *et al.,* 2011).

3.4. Cellular automata simulation

Once trained, the ANN, LR, and RF models were used to simulate future land use through cellular automata (CA), a rule-based probabilistic technique that predicts land use evolution over time (Sarkar, 2000). Transition potential maps from each model, with values ranging from 0 (low change potential) to 1 (high change potential), served as inputs.

Change quantities were determined via the Markov chain approach (Bell, 1974). This produces a transition probability matrix that defines the number of pixels shifting from class *i* to class *j* within the simulation horizon. Spatial allocation of changes was performed using CA. This combined the transition demand from Markov with model transition potentials (Subedi *et al.,* 2013). In each CA iteration, classes competed for each cell. The most suitable class was assigned until the total change for each transition pair was met (Girma *et al.,* 2021; Hamad *et al.,* 2018).

Model accuracy was evaluated through an intermediate validation projecting land use to 2020. Validation included Kappa statistics and minimum total error, comparing simulated and observed 2020 maps. The simulation used 10-year iterations, where the 2000-2010 period represented one iteration.

Additionally, a Kappa index was calculated for pixels that changed between 2010 and 2020. A change mask was created by comparing the two real maps. This mask identified cells that changed categories. It was applied to the simulated 2020 maps from ANN, LR, and RF models, as well as to the actual 2020 map. This focused the analysis only on the changed areas. Using this filtered dataset, per-category Kappa values were calculated. Following Pontius and Millones (2011), quantity disagreement (QD) and allocation disagreement (AD) were also computed to complement the Kappa interpretation (Pontius and Santacruz, 2014).

3.5. Analysis of projected urban expansion implications

After validating the models, projections were created up to 2070. Transition probability matrices from multitemporal analysis were adjusted to three scenarios: (i) a trend scenario subject to ACMUS and non-developable zones (see Figure 2); (ii) an intermediate growth scenario with regulatory changes; and (iii) an accelerated growth scenario without restrictions.

In the trend scenario, ACMUS and non-developable areas remained constraints, reducing the likelihood of conversion to anthropogenic use. The intermediate scenario allowed higher conversion probabilities for natural and agricultural lands, but within regulatory bounds. The accelerated scenario removed all restrictions, increasing conversion rates across categories to reflect high urban pressure (see supplementary material B).

A mask of projected urban expansion under the trend scenario (RF–CA) for 2070 was also created. Within this mask, overlays were applied to temperature and precipitation projections under the climate Shared Socioeconomic Pathways SSP245 (moderate GHG emissions) and SSP585 (high GHG emissions), generated using the IPSL-CM6A-LR global circulation model from WorldClim (Chen *et al.,* 2020). These climate layers were used only for post hoc analysis, not as model inputs. Similarly, a spatial overlay was carried out with the national landslide susceptibility map from the National Risk and Emergency Management Service (SNGR, 2024). The analysis identified areas of projected urban expansion that intersect with risk zones or are vulnerable to climate change. This offers insights into potential consequences for future urban resilience.

It is important to note that climate variables were not included in the simulation process; their integration was exploratory and intended to assess potential conflicts and adaptation opportunities for urban planning.

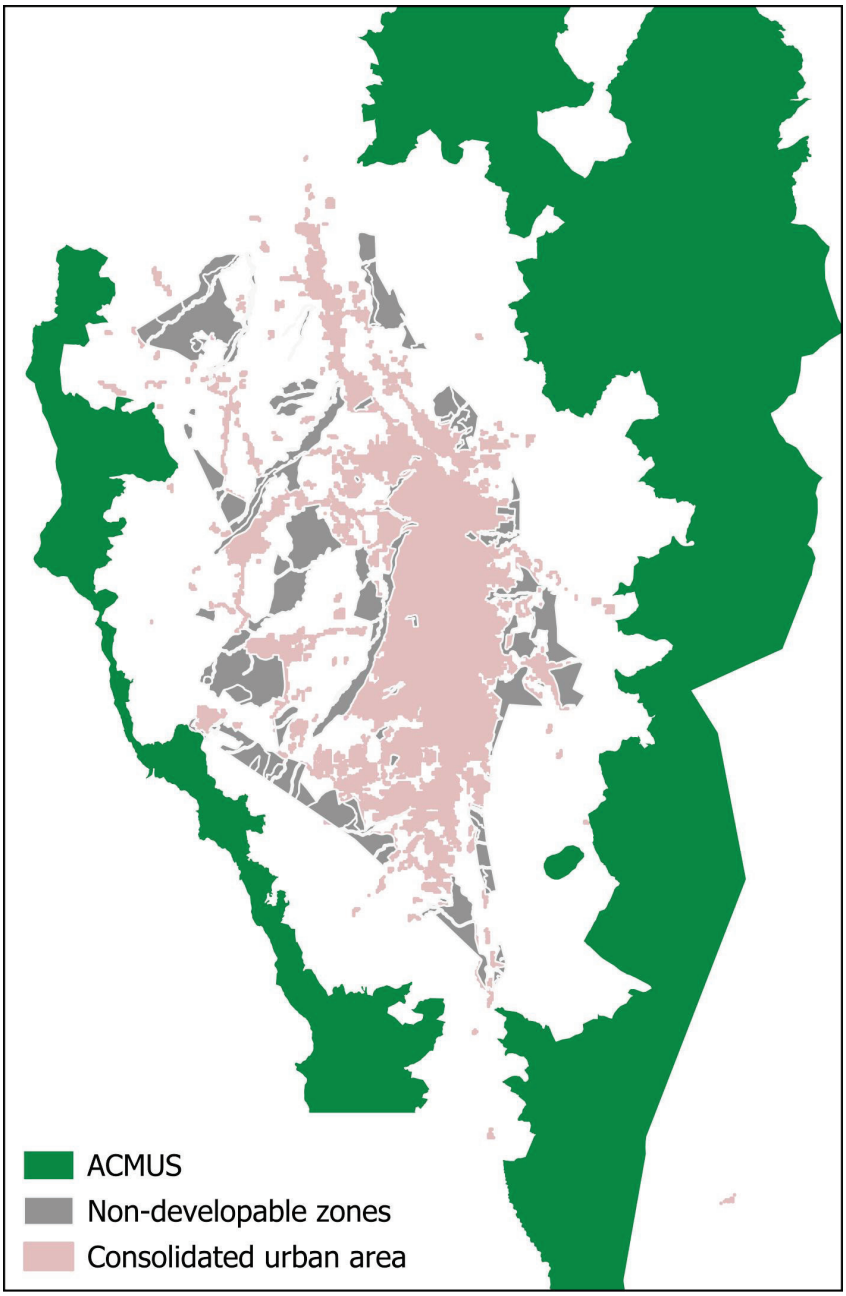

Figure 2. Restrictions used for scenario generation.

4. Results

4.1. Land cover changes (1990-2020)

Land cover analysis between 1990 and 2020 shows substantial transformations across the study area (Fig. 3). Forest cover increased steadily from 33.48% in 1990 to 36.58% in 2020, suggesting natural regeneration processes or effective conservation strategies. In contrast, other natural vegetation declined from 14.39% to 11.43% during the same period.

Agricultural land showed notable fluctuations: it represented 49.14% in 1990, rose slightly to 49.39% in 2000, declined to 46.71% in 2010, and partially recovered to 47.51% in 2020. These variations reflect processes of agricultural intensification or the abandonment of productive land. Anthropogenic areas grew continuously from 2.61% in 1990 to 4.17% in 2020, reflecting urban expansion and population growth. Water bodies decreased gradually from 0.07% in 1990 to 0.01% in 2020, mainly due to urban expansion over natural channels.

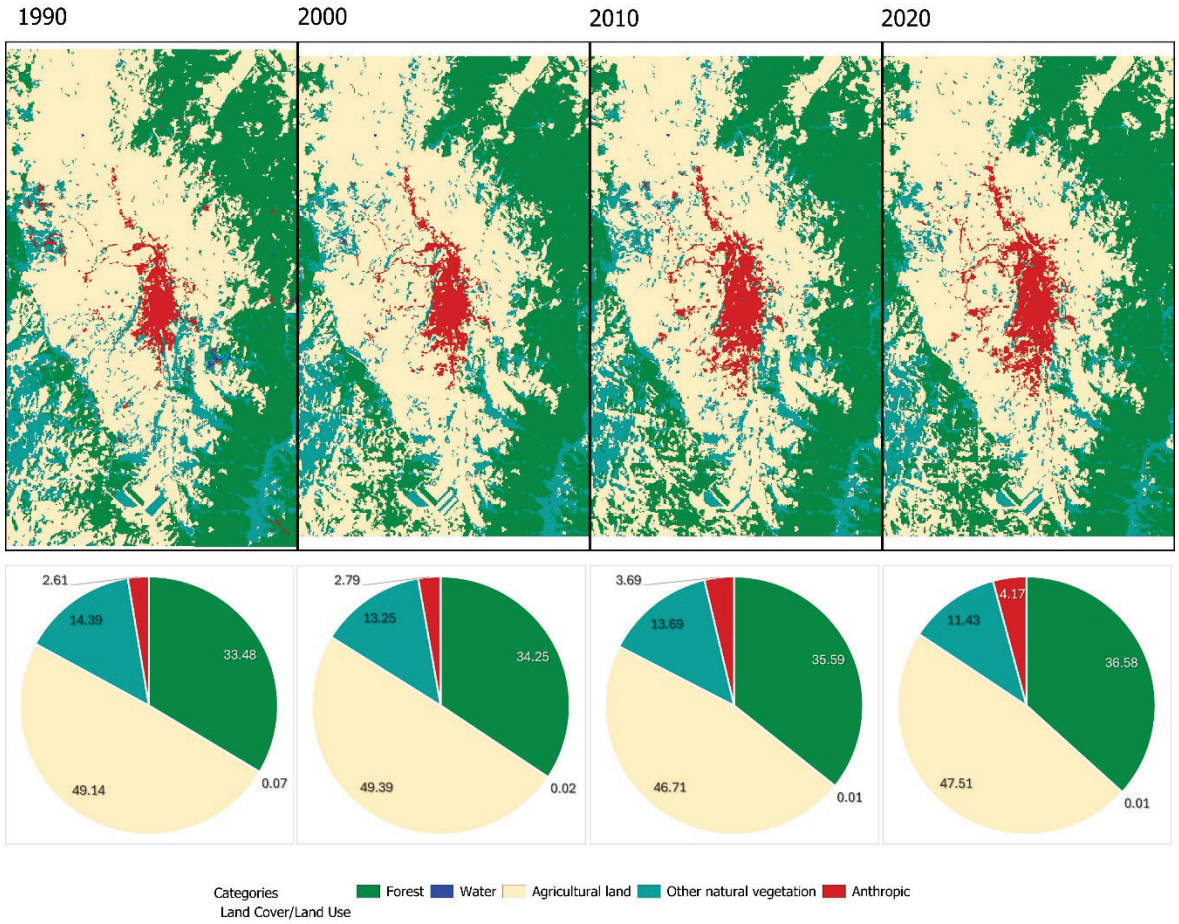

Figure 3. Land cover changes in Loja from 1990 to 2020.

Transition matrices (see supplementary material) reveal conversion patterns among land use categories. Forest gained area mainly at the expense of other natural vegetation, indicating ecological succession, but also lost minor areas to agricultural and urban uses. Agricultural land was the most dynamic class, showing both losses and gains. A significant conversion occurred from other natural vegetation to cropland and pastures, while some agricultural areas reverted to secondary vegetation and forest. Urban expansion occurred primarily over agricultural land, highlighting the conversion of farmland and grazing areas into built-up zones.

Change intensity analysis at the interval level showed that the annual change rate (S_t) peaked between 2000 and 2010, exceeding the uniform intensity line (U), indicating an active change period (see supplementary material D). In contrast, 1990–2000 and 2010–2020 showed lower intensities than U, reflecting latent change dynamics (Fig. 4).

At the category level (Fig. 5), anthropogenic use showed gain intensities above S_t in all three intervals, indicating consistent activity. Agricultural use showed latent gains throughout and active losses only in 2000-2010. Forest exhibited both latent gains and losses across all intervals, indicating low overall change intensity. Other natural vegetation had active gains and losses in all intervals, making it the most dynamic category. Water showed active gains and losses across all periods, although these results should be interpreted cautiously, given this category's limited area.

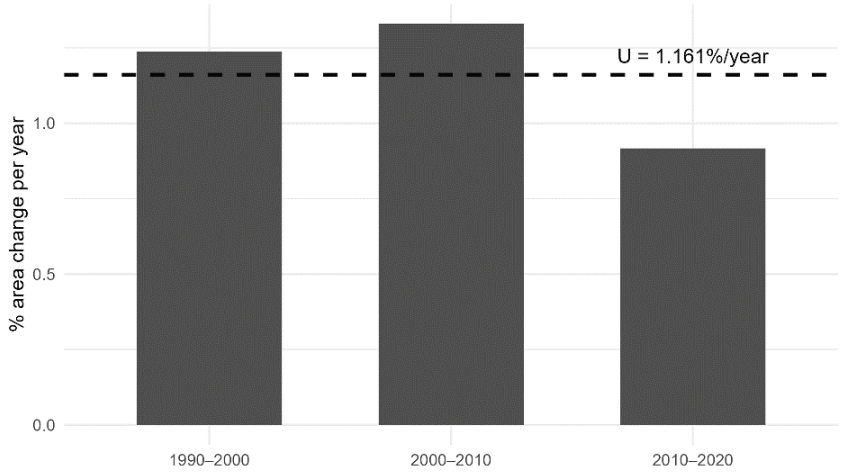

Figure 4. Annual change intensity (S_t) and uniform intensity line (U) for 1990–2020.

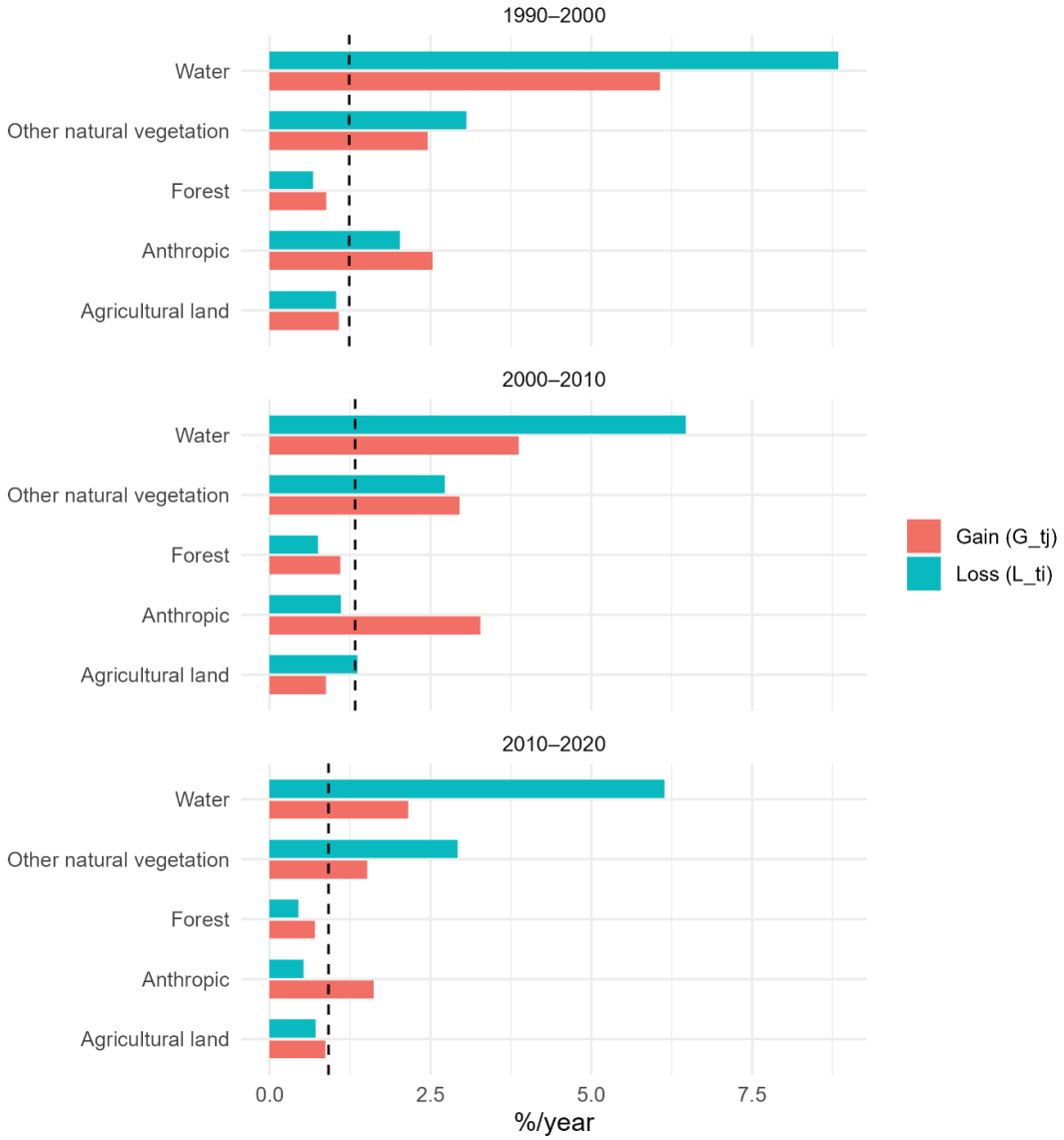

Figure 5. Combined gain and loss intensity by category, relative to S_t.

At the transition level (Fig. 6), the agricultural to anthropogenic transition (land shifting from agricultural to human-developed use) was the most active across all intervals. Here, the observed transition rate (R_{tin}) was greater than the expected uniform rate (W_{tn}), indicating a sustained conversion trend. The water-to-anthropogenic transition (conversion of water bodies to human-developed land) was active in 1990-2010 but was avoided in 2010-2020. This is likely due to the small surface area. Transitions from forest to anthropogenic and other natural vegetation to anthropogenic did not exceed the uniform intensity line. This means the rate did not surpass what would be expected if the change were distributed evenly.

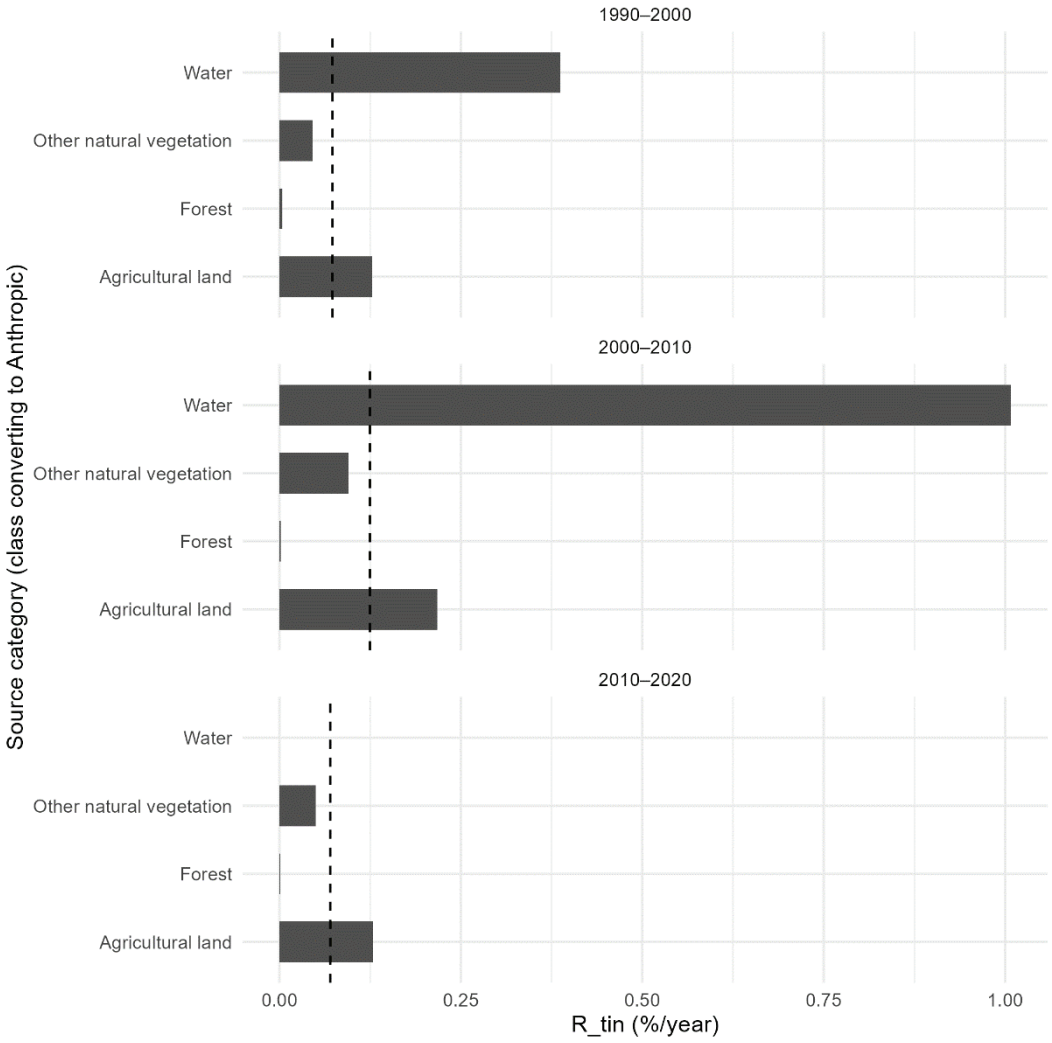

Figure 6. Transition intensities toward anthropogenic use relative to S_t for each time interval.

4.2. Explanatory variables: correlation and importance

The correlation matrix showed the highest coefficients between distance to urban facilities and slope (r = 0.48), and between urban facilities and elevation (r = 0.47). Although these values do not exceed the 0.7 collinearity threshold, they suggest some redundancy that could affect regression model stability. The remaining correlations, ranging from −0.3 to 0.3, indicate weak to moderate relationships, confirming that most variables lack strong dependencies that justify exclusion (Table 3).

Table 3. Pearson correlation matrix among explanatory variables.

Variable	Urban facilities	Migration	Vegetation greenness	Hydrographic network	Road network	Slope	Elevation	Population density
Urban facilities	-	-0.09	0.30	0.10	-0.19	0.48	0.47	-0.31
Migration		-	-0.29	-0.11	0.22	-0.19	-0.21	0.41
Vegetation greenness			-	0.12	-0.16	0.27	0.30	-0.46
Hydrographic network				-	-0.15	0.09	0.21	-0.13
Road network					-	-0.11	-0.15	-0.20
Slope						-	0.33	-0.29
Elevation							-	-0.23
Population density								-

The Cramer's V index showed that the most influential variables for the transition to anthropogenic use were population density (0.75) and distance to road network (0.74), followed by distance to urban facilities (0.68) and slope (0.62). Among biophysical factors, elevation (0.59) and NDVI (0.47) highlight the influence of topography and vegetation cover on urban development patterns.

Internal correlations provided further insight: NDVI correlated positively with slope (r = 0.27) and elevation (r = 0.30), suggesting that vegetated areas tend to occur in higher, steeper terrains where urban pressure is lower. The road network was negatively correlated with NDVI (r = −0.16), indicating that proximity to infrastructure reduces vegetation cover. Migration correlated negatively with NDVI (r = −0.29), slope (r = −0.19), and elevation (r = −0.21), indicating that migrant populations tend to settle in flatter, less vegetated areas suitable for urbanization. The hydrographic network correlated positively with elevation (r = 0.21), reflecting better preservation of these resources in higher, less accessible zones. Population density was higher in low-lying, less vegetated areas, consistent with urban concentration patterns.

4.3 Simulation Model Evaluation and Kappa by Category

ANN and RF models showed high agreement in predicting 2020 land use, while LR showed substantial agreement. Random Forest (RF) achieved the highest overall accuracy (90.72%) and Kappa index (0.852), followed by ANN (0.844) and LR (0.798). By category, RF maintained consistent performance, with Kappa values ranging from 0.853 to 0.906, whereas LR performed less accurately in smaller categories (Table 4).

Table 4. Kappa index by category for land use simulation models.

Category	Kappa ANN	Kappa LR	Kappa RF
Forest	0.896628	0.858356	0.906883
Water	0.777752	0.777755	0.888883
Agricultural land	0.807136	0.773074	0.873822
Other natural vegetation	0.823758	0.721090	0.853912
Anthropic	0.836280	0.803939	0.857769

When analyzing only pixels that changed between 2010 and 2020 (Table 5), the anthropogenic category achieved the highest Kappa values in all models—0.933 for RF, 0.912 for ANN, and 0.838 for LR—showing strong spatial agreement between simulated and observed urban expansion. RF also had the highest overall Kappa (0.69), with low quantity disagreement (QD = 0.04) and allocation disagreement (AD = 0.17). This confirms RF's superior predictive ability for urban growth, while ANN and LR exhibited higher spatial disagreement, particularly in change location.

As shown in Figure 7, ANN, LR, and RF models produced different spatial patterns compared with the observed 2020 data. RF achieved the best spatial fit, especially for "water" and "anthropogenic" categories. ANN tended to overestimate "water" and "other natural vegetation" and excessively fragment "forest." LR accurately estimated the total anthropogenic area (4.18% observed vs. 4.19% projected) but poorly represented its spatial distribution, underestimating urban expansion in the city's southern sector.

Table 5. Kappa by category and disagreement metrics for pixels that changed between 2010 and 2020.

Model	Overall Kappa	Kappa Forest	Kappa Water	Kappa Agricultural land	Kappa Other natural vegetation	Kappa Anthropic	QD*	AD**
ANN	0.59	0.69	0.78	0.43	0.58	0.91	0.07	0.21
LR	0.54	0.60	0.78	0.41	0.48	0.84	0.05	0.28
RF	0.69	0.72	0.91	0.58	0.65	0.93	0.04	0.17

*QD is the quantity disagreement, representing the difference between the simulated and observed amount of change, regardless of its location.

**AD is the allocation disagreement, reflecting the portion of error due to the incorrect spatial location of change, assuming the total amount is correct.

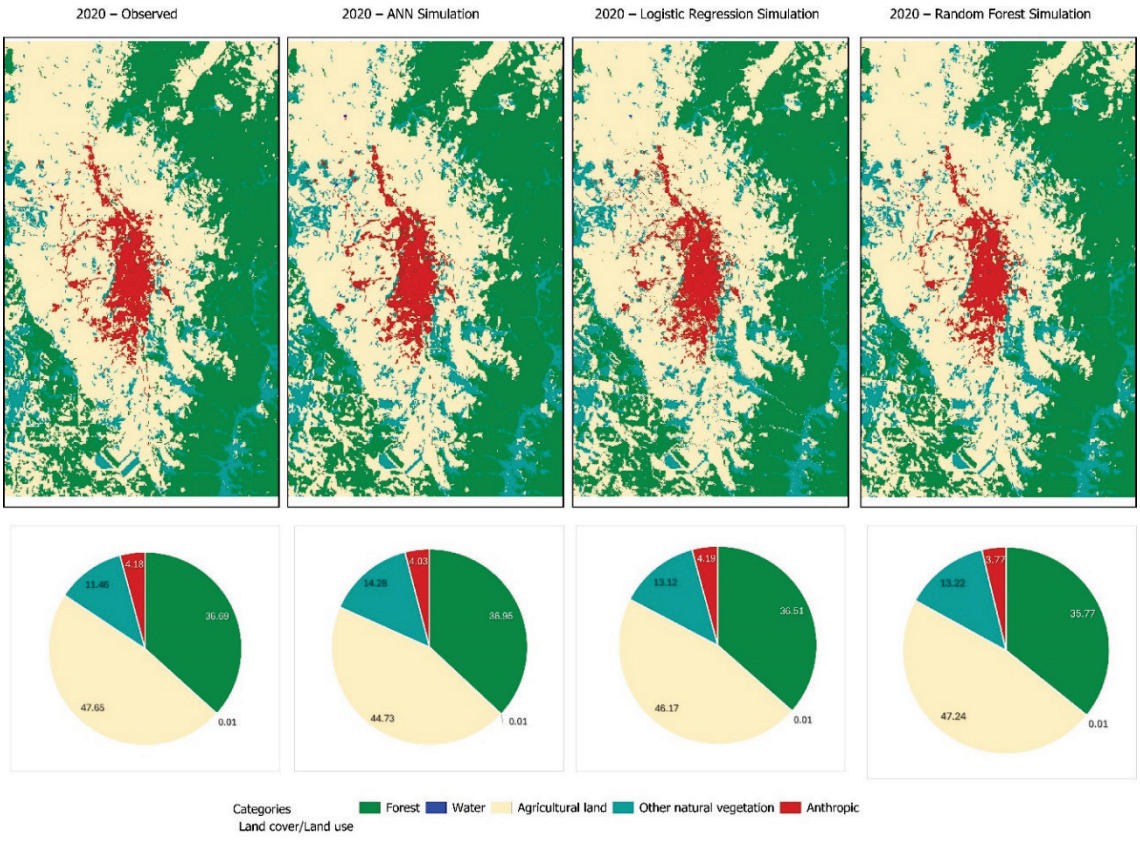

Figure 7. Land cover projection for 2020 using ANN, RF, and LR models.

4.4. Future Projections (2070)

Projected surface variations to 2070 relative to 2020 show that anthropogenic use increases in all scenarios: +20.11% in the trend (RF) scenario, +16.35% in the restricted trend (ACMUS and non-developable zones; see Figure 2), +91.33% in the intermediate growth with regulations, and +171.58% in the accelerated growth without restrictions. Agricultural land decreases by −0.70%, −3.85%, −7.78%, and −11.71%, respectively. Forest also decreases in all scenarios, with reductions of −0.90%, −2.68%, −4.63%, and −7.55%, showing more substantial declines as restrictions are relaxed and urban pressures intensify (Table 6).

In percentage terms, the water category increases slightly across scenarios, though it represents a small portion of the total area. The spatial distribution of the four scenarios is shown in Figure 8.

Table 6. Projected surface area by category and scenario for 2070

Category	2020	2070 Trend (RF)	2070 Trend with restrictions	2070 Intermediate growth with restrictions	2070 Accelerated growth without restrictions
Forest	15,699.72	15,559.20	15,279.03	14,973.39	14,514.93
Water	2.50	4.77	5.04	5.04	5.04
Agricultural land	20,389.19	20,246.40	19,605.15	18,803.52	18,001.80
Other natural vegetation	4,905.50	4,836.51	5,825.07	5,589.81	5,413.41
Anthropic	1,790.32	2,150.37	2,082.96	3,425.49	4,862.07

Note: The areas are expressed in hectares. The restrictions correspond to the limits of the ACMUS and non-developable zones as defined in the current PDOT.

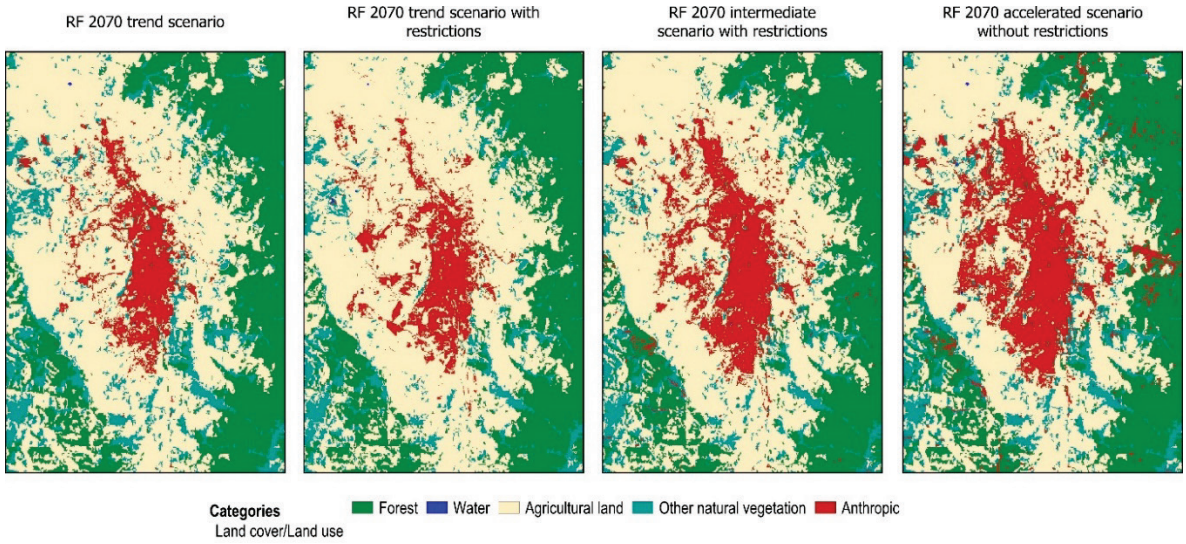

Figure 8. Land cover projection to 2070 using Random Forest (RF) simulation model.

4.5. Climate Implications of Projected Urban Expansion to 2070

The climate assessment was performed only for the 2070 trend scenario (RF–CA). Projections (Fig. 9) indicate that most of urban expansion is expected to occur over agricultural land (93.6%), followed by a smaller proportion affecting other natural vegetation (6.15%), and minimal conversion from forest and water. These results reveal a pattern of transformation of agricultural and natural ecosystems into urban areas. Moreover, 41.9% of the expansion would occur in low-risk zones, 17.2%

in high-risk zones, and 40.9% in medium-risk zones, increasing exposure to climate hazards. At the parish level, Sucre leads urban expansion (41.3%), followed by Punzara (24.3%) and Carigán (11.1%). In comparison, 10.6% of new urban areas would extend beyond the current urban perimeter, underscoring the need for planning regulations.

Figure 10 shows current and projected distributions of temperature and precipitation under the SSP245 and SSP585 scenarios. Under SSP245, temperature is projected to rise by an average of 1.3 °C, with precipitation increasing by about 50 mm. SSP585 projects more severe changes, including temperature increases of up to 4 °C and precipitation increases of up to 150 mm, which could exacerbate heat stress, flooding, and water scarcity.

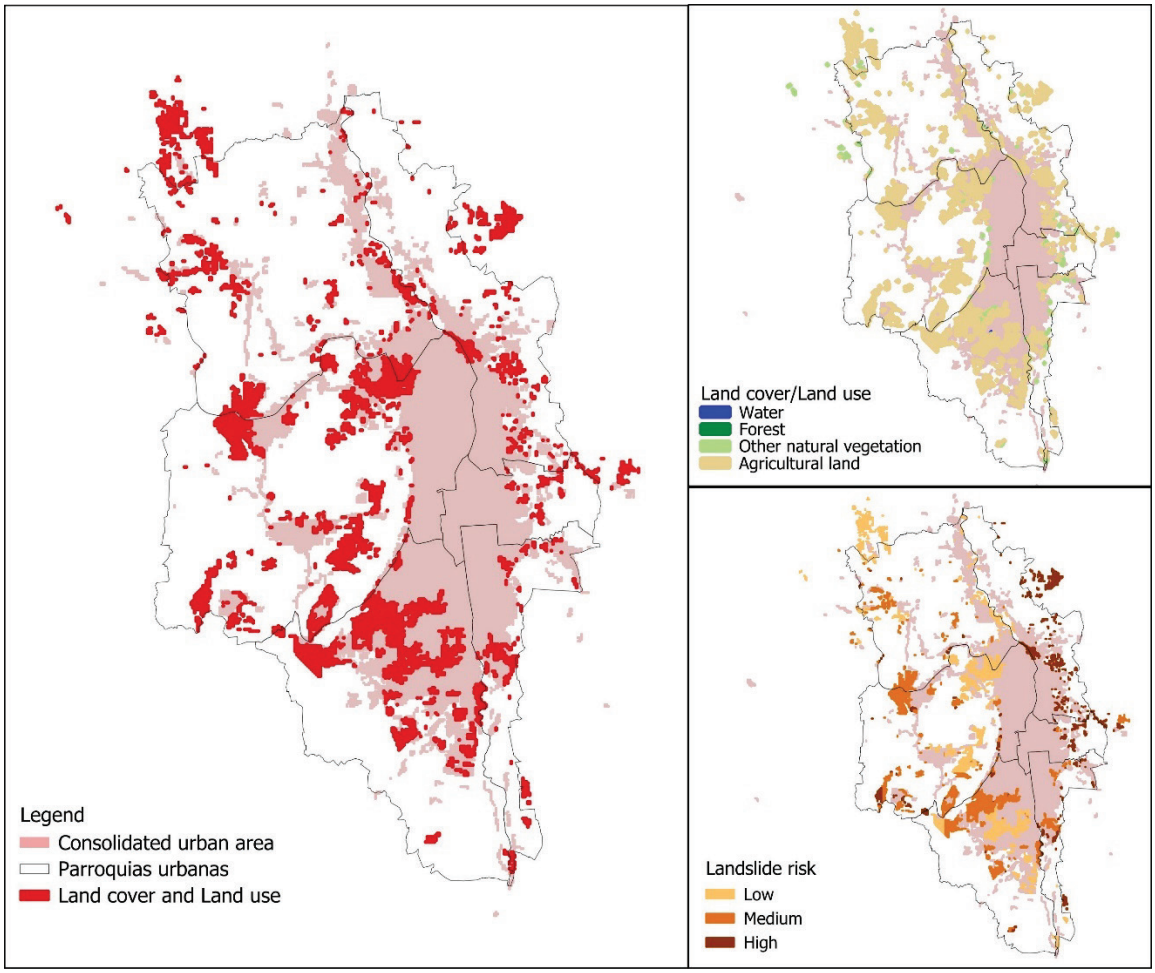

Figure 9. Projected urban expansion to 2070 using RF simulation, categorized by land use and landslide risk level.

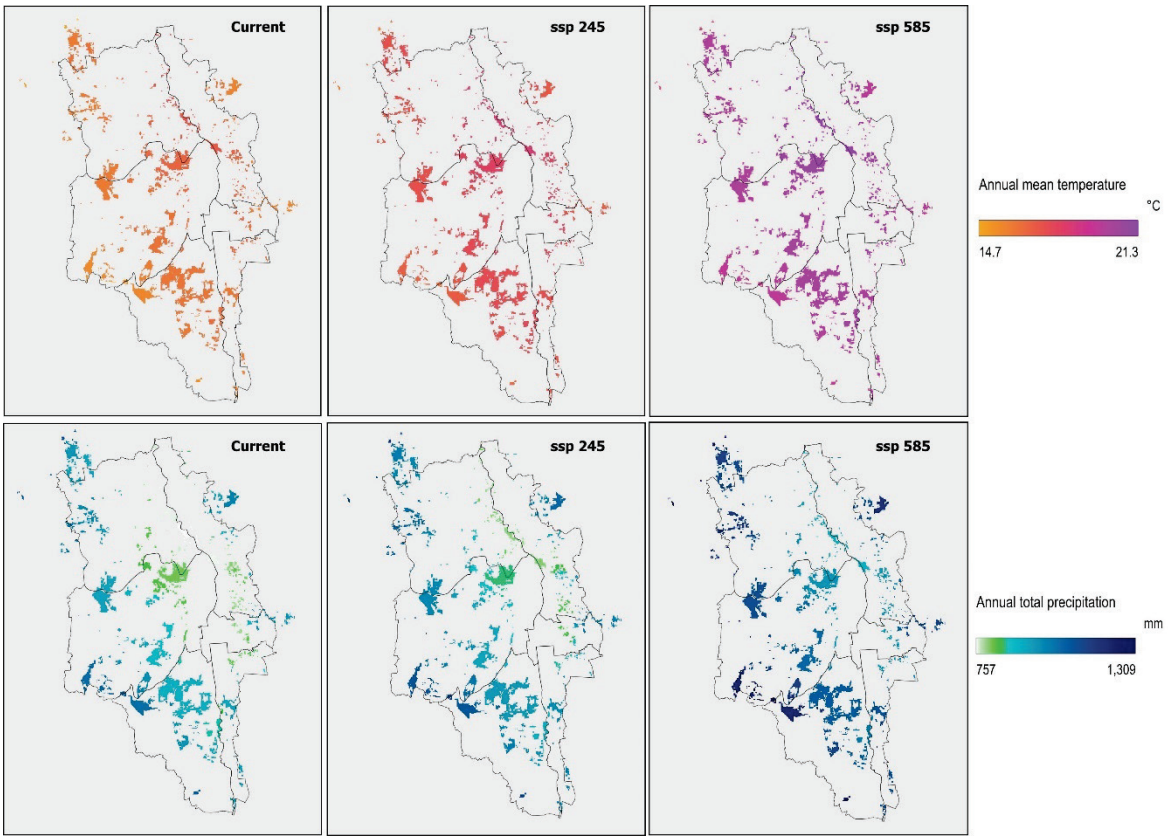

Figure 10. Projected 2070 urban expansion and ranges of temperature and precipitation.

4.5.1. Land Use and Climate Projections

The overlay between land-use projections and future temperature and precipitation distributions shows that urban expansion in "water" and "other natural vegetation" areas corresponds to the lowest temperature ranges (16.3-20.3 °C). On the other hand, "forest" and "agricultural land" show slightly higher values (up to 20.5 °C). Urban occupation of forested or agricultural zones could therefore intensify the urban heat island effect. In terms of precipitation, "water" areas receive the highest annual rainfall (912-1075 mm), followed by "other natural vegetation" and "agricultural land" (894-1069 mm). Expansion over water bodies will require robust flood management infrastructure, while forest areas may face water scarcity risks.

4.6. Differences by Risk Level

Risk-level analysis shows that high-risk zones have higher temperatures (16.6-20.5 °C) and lower precipitation (830-983 mm) compared with low-risk areas (16.4-20.4 °C and 886-1102 mm, respectively). This suggests that urban expansion into high-risk zones would increase exposure to extreme heat and drought. Conversely, low-risk areas offer more favorable conditions for sustainable urban development.

4.7. Differences by Parish

By parish, Punzara exhibits the lowest temperatures (15.4-20.5 °C) and highest precipitation (862-1075 mm), implying the need for adequate water management infrastructure. Carigán shows the highest temperatures (16.7-21.2 °C) and lowest precipitation (764-987 mm), reflecting higher thermal stress and water scarcity. Sagrario and Sucre present intermediate conditions, with moderate

temperatures and relatively high precipitation, making them more balanced climatically. Areas outside the current urban perimeter represent about 10% of the projected expansion. These areas have the highest precipitation in both SSP245 and SSP585 scenarios, making them vulnerable due to limited infrastructure and services.

5. Discussion

5.1. Land Use Dynamics and Projections in Loja

This analysis addresses a critical gap in understanding urban growth in Loja by integrating advanced simulation models with key components of sustainable development, including climate projections and risk zones.

Results indicate that between 1990 and 2020, agricultural areas decreased by approximately 700 hectares, while urbanized areas increased by 668 hectares. The change intensity analysis revealed its highest rate during 2000-2010 (S_t = 1.329%/year > U = 1.161%/year), followed by active change in 1990–2000 (1.238%/year) and latent change in 2010–2020 (0.916%/year). By category, the anthropogenic zone consistently showed active gains (G_{tj} = 2.536, 3.274, and 1.614%/year, all > S_t), indicating sustained urban demand. Agricultural land showed active losses only in 2000–2010 (L_{ti} = 1.367%/year > S_t) and latent losses in 1990-2000 and 2010-2020 (1.036 and 0.714%/year < S_t), confirming that this category contributes most to urban expansion. Forest maintained latent gains and losses across all intervals (G_{tj} = 0.885, 1.100, 0.708 and L_{ti} = 0.676, 0.751, 0.450%/year, all < S_t), consistent with biophysical and regulatory constraints that limit deforestation. Other natural vegetation was the most dynamic category (G_{tj} = 2.457, 2.958, 1.521 and L_{ti} = 3.058, 2.723, 2.920%/year, all > S_t), consistent with ecological succession, land abandonment, and peri-urban reconversion processes.

Overall, the main pattern identified is the accelerated conversion of agricultural land into urban areas, aligning with global findings such as those by Bren d'Amour *et al.* (2016), who emphasize the global impact of urban expansion on croplands.

5.2. Performance of the Simulation Models

All three simulation models projected urban expansion toward 2020. However, the hybrid model combining Random Forest (RF) with Cellular Automata (CA) proved the most accurate, achieving a Kappa index of 0.852 and an overall accuracy of 90.72%, outperforming Artificial Neural Networks (ANN) and Logistic Regression (LR). The validation based on pixels with actual changes confirmed that all models perform best when simulating the location and extent of new urban areas. In contrast, agricultural and natural vegetation categories showed lower Kappa values due to their high spatial and temporal variability (see transition matrices in the supplementary material C and D).

Disagreement metrics provided additional insight: quantity disagreement (QD) and allocation disagreement (AD) differentiated whether errors arose from differences in change magnitude or spatial allocation, thus overcoming one of the limitations of the Kappa index (Pontius and Millones, 2011).

Integrating RF with CA captured both the spatial and temporal dynamics of urban growth (Gaur and Singh, 2023). According to Kamusoko and Gamba (2015), hybrid models combining RF improve prediction accuracy. These models can handle large, heterogeneous datasets and model complex interactions among explanatory variables such as road accessibility, proximity to urban facilities, and topographic conditions. Topography and existing urban infrastructure have also been identified as key drivers of expansion (Herold *et al.,* 2003; Sakieh, 2015; Schuster-Olbrich *et al.,* 2024). Furthermore, Mutale *et al.* (2024) highlight that this approach reduces overfitting, making it especially useful in areas with high spatial variability, such as Loja.

5.3. Future scenario projections

Projections indicate that by 2070, urban expansion will occur mainly on agricultural land (93.6%) and to a lesser extent on natural vegetation (6.15%), with minimal conversion of forests (0.216%) and water bodies (0.038%). Approximately 41.9% of urban growth is expected in low-risk zones, while 17.2% will occur in high-risk areas. These trends align with findings by Krivoguz (2024) on the Kerch Peninsula, where urbanization has transformed farmland, and by Thomas *et al.* (2024), who highlights territorial fragmentation and rising climate vulnerability in Latin American cities driven by unregulated urban growth.

Despite the robustness of the applied methodology, some limitations remain. The lack of high-resolution data in intermediate cities like Loja affects projection precision. Mapping small water bodies is particularly difficult, as narrow rivers and streams fall below the 30 m pixel resolution. The observed decline in this category aligns with historical processes such as channelization and culverting of streams to enable urban expansion, as well as the restoration of certain streambeds, which may explain transitions from water to forest cover.

Although the RF–CA hybrid model proved effective, its reliance on specific variables may not fully capture the complexity of the socioeconomic and environmental drivers influencing land-use change. Hagenauer *et al.* (2019) note that selecting an optimal model remains challenging because results depend on context and data quality. Therefore, future scenario models should incorporate constraints such as municipal ordinances (local laws governing land use), protected areas, and conservation policies (Gaur and Singh, 2023). These variables are essential to produce realistic scenarios by guiding or limiting urban expansion.

In the generated 2070 scenarios, municipal conservation areas (ACMUS) and other regulated zones restricted urban growth, while new infrastructure and economic incentives directed it toward specific areas. The trend and restricted trend scenarios differ in magnitude (+20.11% vs. +16.35%, respectively) but not in spatial pattern, as no expansion occurs within ACMUS. This outcome is consistent with the long-standing protection of the eastern and western slopes, designated as protected forests and water catchment areas decades ago (United Nations Environment Programme [UNEP] *et al.*, 2007). This historical protection explains the persistence of a stable peri-urban forest belt around Loja, confirming the effectiveness of local regulations.

Incorporating these constraint variables in future studies would enhance simulation accuracy and applicability. The moderate correlation between distance to facilities and slope suggests that urban growth tends to concentrate in well-serviced, accessible areas, confirming the role of basic infrastructure in shaping new development.

5.4. Implications for Urban Planning

The findings carry significant implications for sustainable urban planning. First, expansion should prioritize areas with lower temperatures and moderate rainfall, such as Punzara parish. This implies limiting growth in Sucre, where the model projects the highest concentration of expansion. Even in favorable areas, infrastructure is needed to manage flood risks and extreme precipitation events.

Second, it is crucial to prevent more than 50% of future expansion from occurring in medium- and high-risk zones characterized by high temperatures and low rainfall, as these conditions may intensify climate impacts. Urban heat mitigation strategies—such as green roofs, reflective pavements, and shaded public spaces—should be implemented, particularly in warmer areas. In recent years, solutions such as green and blue infrastructure, sponge-city systems (Gündel *et al.,* 2023), and cooling strategies have attracted attention for reducing thermal stress and heat-related health risks (Guillén and Orellana, 2016; Katzschner, 2011; Li *et al.,* 2024).

Third, the projected decline in shrub and agricultural areas suggests pressure on productive landscapes. According to van Berkum (2023), croplands in the Global South often follow two trajectories: intensification or displacement to more distant zones due to rising land prices. In Loja, urban expansion advances over agricultural areas, yet several agricultural patches persist in peri-urban zones, suggesting the potential to maintain domestic food production even under urbanization. Integrating these peri-urban agricultural practices into land-use planning can enhance food security and climate resilience.

Unregulated urban growth degrades conservation soils, which are essential for water recharge and biodiversity. Water management is key not only to secure supply during droughts but also to manage runoff during intense rainfall. While forests have gained area, their distribution remains peripheral, likely due to natural regeneration rather than reforestation programs. Maintaining forest cover in high-rainfall zones supports drainage and water absorption (Ponte *et al.,* 2024).

Projected growth also raises concerns about socioeconomic vulnerability. By mid-century, most population growth will occur in developing-country cities, increasing land demand and property values (van Berkum, 2023). Rising land costs drive informal settlements, often located in hazardous areas (Lazcano Martínez, 2005). In Loja, 40.6% of informal settlements are located in medium-risk zones and 34.7% in high-risk areas, heightening their vulnerability. Addressing this issue requires proactive planning measures and stronger governance.

Urban expansion is inevitable; the challenge lies not in containment but in ensuring socially just and environmentally safe growth. Sustainable urban development depends on managing expansion equitably, directing it toward safe areas, protecting environmental assets, and ensuring accessibility for all socioeconomic groups.

6. Conclusions

The 2000-2010 period was selected for calibration because explanatory variables were available for that decade. All variables were spatially standardized (30 m resolution, same projection) and temporally anchored to this period, assuming relative stability in urban dynamics. Although this approach introduces some temporal heterogeneity, the Random Forest–CA model achieved strong performance (Kappa = 0.856; AD = 0.17; anthropogenic category Kappa = 0.933), indicating that the selected variables effectively captured spatial patterns of urban growth. Future studies could improve accuracy by synchronizing variable years or performing sensitivity analyses on temporal anchoring.

In this case study, the most influential variables driving land use change and urban growth were distance to infrastructure (facilities and major roads), population dynamics (migration in 2001 and population density in 2010), and topography. These findings confirm that urban growth is not random but concentrated in well-serviced, accessible areas with moderate slopes. The correlation between facilities and slope (r = 0.48) suggests that as infrastructure expands, urban development tends to occur on steeper slopes. If this trend continues, 17.2% of the projected expansion by 2070 will occur in high landslide-risk areas, where over 34% of informal settlements already exist. Therefore, territorial planning must prioritize risk zoning, strengthen local governance to prevent settlement in vulnerable zones, and adopt nature-based solutions to reduce landslide susceptibility.

By calibrating models with 2000–2010 transitions and validating against 2020 land use, the hybrid RF–CA model achieved the highest precision (Kappa = 0.86), outperforming ANN and LR. For this case, RF proved best at handling nonlinear relationships and minimizing overfitting, making it a reliable tool for urban expansion scenario planning.

Projected urban expansion by 2070 will primarily affect agricultural (93.6%) and natural vegetation areas (6.15%), implying significant losses of land crucial for food security, biodiversity, and ecosystem regulation. Historical transition and intensity analyses (1990–2020) revealed that conversion

from agricultural to urban land is the most active and preferred change type, with an accumulated loss of around 700 ha of farmland. Sustained urban pressure reduces peri-urban productivity and threatens food security. Strengthening the management of Municipal Conservation and Sustainable Use Areas (ACMUS) is thus essential—not only for conservation but also for promoting peri-urban agriculture and food resilience under climate change.

The applied methodology—integrating machine learning models, change intensity analysis, spatial simulation, and climate risk assessment—is replicable in other Latin American intermediate cities with limited data. This combined approach provides robust evidence for spatial planning and should be incorporated into future land-use and risk management plans to promote sustainable territorial development.

Acknowledgments

The authors thank the Ecuadorian Corporation for the Development of Research and Academia (CEDIA) for financial support through the R&D&I Fund for Universities, within the project *I+D+I-XVIII-2023-48-APTEcuCC: Analysis of Territorial Problems in Ecuador Using Machine Learning and Remote Sensing from a Climate Change Perspective*.

References

Aldwaik, S.Z., Pontius, R.G., 2012. Intensity analysis to unify measurements of size and stationarity of land changes by interval, category, and transition. *Landscape and Urban Planning* 106(1), 103–114. https://doi.org/10.1016/j.landurbplan.2012.02.010

Allan, A., Soltani, A., Abdi, M.H., Zarei, M., 2022. Driving Forces behind Land Use and Land Cover Change: A Systematic and Bibliometric Review. *Land* 11(8), 1222. https://doi.org/10.3390/land11081222

Alshari, E.A., Gawali, B.W., 2022. Modeling Land Use Change in Sana'a City of Yemen with MOLUSCE. *Journal of Sensors 2022*, 1–15. https://doi.org/10.1155/2022/7419031

Alsharif, A. a. A., Pradhan, B., 2013. Urban sprawl analysis of Tripoli Metropolitan City (Libya) using remote sensing data and multivariate logistic regression model. *Journal of the Indian Society of Remote Sensing* 42(1), 149–163. https://doi.org/10.1007/s12524-013-0299-7

Bell, E.J., 1974. Markov analysis of land use change—An application of stochastic processes to remotely sensed data. *Socio-Economic Planning Sciences 8*(6), 311–316. https://doi.org/10.1016/0038-0121(74)90034-2

Bell, S., Alves, S., de Oliveira, E.S., Zuin, A., 2010. Migration and land use change in Europe: A review. *Living Reviews in landscape research*, *4*.

Bren d'Amour, C., Reitsma, F., Baiocchi, G., Barthel, S., Güneralp, B., Erb, K.-H., Haberl, H., Creutzig, F., Seto, K.C., 2017. Future urban land expansion and implications for global croplands. *Proceedings of the National Academy of Sciences of the United States of America* 114(34), 8939–8944. https://doi.org/10.1073/pnas.1606036114

Chen, G., Li, X., Liu, X., Chen, Y., Liang, X., Leng, J., Xu, X., Liao, W., Qiu, Y., Wu, Q., Huang, K., 2020. Global projections of future urban land expansion under shared socioeconomic pathways. *Nature Communications 11*(1). https://doi.org/10.1038/s41467-020-14386-x

Deng, Z., Quan, B., 2022. Intensity Characteristics and Multi-Scenario projection of land use and land cover change in Hengyang, China. *International Journal of Environmental Research and Public Health 19*(14), 8491. https://doi.org/10.3390/ijerph19148491

Faheem, Z., Kazmi, J.H., Shaikh, S., Arshad, S., Noreena, N., Mohammed, S., 2024. Random forest-based analysis of land cover/land use LCLU dynamics associated with meteorological droughts in the desert ecosystem of Pakistan. *Ecological Indicators* 159, 111670. https://doi.org/10.1016/j.ecolind.2024.111670

FIC (Fundación para la Investigación del Clima), Lavola S.A., Universidad Técnica Particular de Loja, 2021. *Índice de Vulnerabilidad al Cambio Climático y Plan de Adaptación para la ciudad de Loja, Ecuador.* Resumen ejecutivo. Caracas: CAF. Retrieved from https://scioteca.caf.com/handle/123456789/1812

Gallardo, M., 2018. Revisión y Análisis de estudios de Modelos de Cambios de Uso del Suelo y de Escenarios a Futuro. *Geographicalia* 70, 1-26

Gao, C., Cheng, D., Iqbal, J., Yao, S., 2023. *Spatiotemporal Change Analysis and Prediction of Future Land Cover Changes Using QGIS MOLUSCE Plugin on a Large Regional Scale and the Relationship Analysis with Mountain Hazards: A Case Study of the Great Yellow River Region (GYRR).* China. Land.

Gaur, S., Singh, R., 2023. A Comprehensive Review on Land Use/Land Cover (LULC) Change Modeling for Urban Development: Current Status and Future Prospects. *Sustainability* 15(2), 903. https://doi.org/10.3390/su15020903

Girma, R., Fürst, C., Moges, A., 2021. Land use land cover change modeling by integrating artificial neural network with cellular Automata-Markov chain model in Gidabo river basin, main Ethiopian rift. *Environmental Challenges 6*, 100419. https://doi.org/10.1016/j.envc.2021.100419

Gobierno de Ecuador, 2024a. *Eventos peligrosos* [Conjunto de datos]. Datos Abiertos Ecuador. https://www.datosabiertos.gob.ec/dataset/eventos-peligrosos/resource/1e170a6f-7f6e-48a3-a46b-be97c265fb1b

Gobierno de Ecuador, 2024b. *Plan de Desarrollo para el Nuevo Ecuador 2024-205. Eje de Riesgos.* Secretaría Nacional de Planificación y Secretaría Nacional de Gestión de Riesgos. https://www.planificacion.gob.ec/wp-content/uploads/2024/05/PND24-25Eje5.pdf

Guillén, V., Orellana, D., 2016. *Un acercamiento a caracterizar la isla de calor en Cuenca, Ecuador.* CONAMA, 2016.

Gündel, H., Önaç, A.K., 2023. *Sponge City Based on Blue – Green Urbanism*. https://doi.org/10.52460/issc.2023.053

Gündüz, H.İ., 2025. Land-Use Land-Cover Dynamics and Future Projections Using GEE, ML, and QGIS-MOLUSCE: A Case Study in Manisa. *Sustainability* 17(4), 1363. https://doi.org/10.3390/su17041363

Hagenauer, J., Omrani, H., Helbich, M., 2019. Assessing the performance of 38 machine learning models: the case of land consumption rates in Bavaria, Germany. *International Journal of Geographical Information Science* 33(7), 1399–1419. https://doi.org/10.1080/13658816.2019.1579333

Hamad, R., Balzter, H., Kolo, K., 2018. Predicting Land Use/Land Cover Changes Using a CA-Markov Model under Two Different Scenarios. *Sustainability 10*(10), 3421. https://doi.org/10.3390/su10103421

Herold, M., Goldstein, N.C., Clarke, K.C., 2003. The spatiotemporal form of urban growth: Measurement, analysis and modeling. *Remote Sensing of Environment 86*(3), 286–302. https://doi.org/10.1016/S0034-4257(03)00075-0

Kafy, A.A., Rahman, M.S., Hasan, M.M., Islam, M., 2020. Modelling future land use land cover changes and their impacts on land surface temperatures in Rajshahi, Bangladesh. *Remote Sensing Applications: Society and Environment* 18, 100314. https://doi.org/10.1016/j.rsase.2020.100314

Kamaraj, M., Rangarajan, S., 2022. Predicting the future land use and land cover changes for Bhavani basin, Tamil Nadu, India, using QGIS MOLUSCE plugin. *Environmental Science and Pollution Research 29*(57), 86337–86348. https://doi.org/10.21203/rs.3.rs-616393/v1

Kamusoko, C., Gamba, J., 2015. Simulating Urban Growth Using a Random Forest-Cellular Automata (RF-CA) Model. *ISPRS International Journal of Geo-Information* 4(2), 447–470. https://doi.org/10.3390/ijgi4020447

Katzschner, L., 2011. Urban Climate Strategies Against Future Heat Stress Conditions. In: Otto-Zimmermann, K. (eds). *Resilient Cities. Local Sustainability*, vol 1. Springer, Dordrecht. https://doi.org/10.1007/978-94-007-0785-6_8

Krivoguz, D., 2024. The Kerch Peninsula in Transition: A Comprehensive Analysis of Land Use and Land Cover Changes Over Thirty Years. Preprint.org. https://doi.org/10.20944/preprints202404.0496.v2

Lazcano Martínez, M., 2005. El acceso al suelo y a la vivienda de los sectores informales: el caso de la ciudad de México. *Revista INVI 20*(54). https://doi.org/10.5354/0718-8358.2005.62171

Leta, M.K., Demissie, T.A., Tränckner, J., 2021. Modeling and Prediction of Land Use Land Cover Change Dynamics Based on Land Change Modeler (LCM) in Nashe Watershed, Upper Blue Nile Basin, Ethiopia. *Sustainability 13*(7), 3740. https://doi.org/10.3390/su13073740

Li, S., Yang, X., Cui, P., Sun, Y., Song, B., 2024. Machine-Learning-Algorithm-Based Prediction of Land Use/Land Cover and Land Surface Temperature Changes to Characterize the Surface Urban Heat Island Phenomena over Harbin, China. *Land 13*(8), 1164. https://doi.org/10.3390/land13081164

Lin, Y., Chu, H., Wu, C., Verburg, P.H., 2010. Predictive ability of logistic regression, auto-logistic regression and neural network models in empirical land-use change modeling – a case study. *International Journal of Geographical Information Science* 25(1), 65-87. https://doi.org/10.1080/13658811003752332

Lu, H., Shang, Z., Ruan, Y., Jiang, L., 2023. Study on Urban Expansion and Population Density Changes Based on the Inverse S-Shaped Function. *Sustainability* 15(13), 10464. https://doi.org/10.3390/su151310464

Lukas, P., Melesse, A.M., Kenea, T.T., 2023. Prediction of future Land Use/Land Cover changes using a coupled CA-ANN model in the Upper Omo–Gibe River Basin, Ethiopia. *Remote Sensing 15*(4), 1148. https://doi.org/10.3390/rs15041148

Mahtta, R., Fragkias, M., Güneralp, B., Mahendra, A., Reba, M., Wentz, E.A., Seto, K.C., 2022. Urban land expansion: the role of population and economic growth for 300+ cities. *Npj Urban Sustainability 2*(1). https://doi.org/10.1038/s42949-022-00048-y

Malek, Ž., Douw, B., Van Vliet, J., Van Der Zanden, E.H., Verburg, P.H., 2019. Local land-use decision-making in a global context. Environmental Research Letters 14(8), 083006. https://doi.org/10.1088/1748-9326/ab309e

MapBiomas, 2025. MapBiomas – *Collection 2.0 of the Annual Series of Land Cover and Land Use Maps of Ecuador (including the Galápagos Archipelago), covering the period 1985–2023.* Consulted on 31 Mar 2025. Available at: https://ecuador.mapbiomas.org/mapas-de-cobertura-y-uso/

Mei, Z., Wu, H., Li, S., 2018. Simulating land-use changes by incorporating spatial autocorrelation and self-organization in CLUE-S modeling: A case study in Zengcheng District, Guangzhou, China. *Frontiers of Earth Science 12*(2), 299–310. https://doi.org/10.1007/s11707-017-0639-y

Ministerio de Desarrollo Urbano y Vivienda (MIDUVI), 2015. *Informe Nacional de Ecuador para la III Conferencia de NNUU sobre vivienda y desarrollo sostenible. Subsecretaría de Hábitat y Asentamientos Humanos* – SHAH.

Mou, J., Chen, Z., Huang, J., 2023. Predicting Urban Expansion to Assess the Change of Landscape Character Types and Its Driving Factors in the Mountain City. *Land* 12(4), 928. https://doi.org/10.3390/land12040928

Muhammad, R., Zhang, W., Abbas, Z., Guo, F., Gwiazdzinski, L., 2022. Spatiotemporal change analysis and prediction of future land use and land cover changes using QGIS MOLUSCE plugin and remote sensing big data: a case study of Linyi, China. *Land* 11(3), 419.

Mutale, B., Qiang, F., 2024. Modeling future land use and land cover under different scenarios using patch-generating land use simulation model. A case study of Ndola district. *Frontiers in Environmental Science 12*. https://doi.org/10.3389/fenvs.2024.1362666

Municipio de Loja, 2020. *Ordenanza Municipal 026-2020 sobre la protección y restauración de fuentes de agua, ecosistemas frágiles, biodiversidad y servicios ambientales del cantón Loja a través de la creación y gestión de áreas de conservación municipal y uso sostenible* -ACMUS.

Municipio de Loja, 2021. Plan de uso y gestión del suelo cantón Loja. https://www.loja.gob.ec/contenido/plan-de-desarrollo-y-ordenamiento-territorial

Nong, Y., Du, Q., 2011. Urban growth pattern modeling using logistic regression. *Geo-spatial Information Science* 14(1), 62–67. https://doi.org/10.1007/s11806-011-0427-x

Ortega-Andrade, H.M., Blanco, M.R., Cisneros-Heredia, D.F., Arévalo, N.G., Vargas-Machuca, K.G.L. de, Sánchez-Nivicela, J.C., Armijos-Ojeda, D., Andrade, J.F.C., Reyes-Puig, C., Riera, A.B.Q., Székely, P., Soto, O.R.R., Székely, D., Guayasamin, J.M., Pesántez, F.R.S., Amador, L., Betancourt, R., Ramírez-Jaramillo, S.M., Timbe-Borja, B., Muñoz, M.H.Y., 2021. Red List assessment of amphibian species of Ecuador: A multidimensional approach for their conservation. *PLOS ONE* 16(5), e0251027. https://doi.org/10.1371/journal.pone.0251027

Ouma, Y.O., Nkwae, B., Odirile, P., Moalafhi, D.B., Anderson, G., Parida, B., Qi, J., 2024. Land-Use Change Prediction in Dam Catchment Using Logistic Regression-CA, ANN-CA and Random Forest Regression and Implications for Sustainable Land–Water Nexus. *Sustainability* 16(4), 1699. https://doi.org/10.3390/su16041699

Ponte, S., Oishi, A.C., Sonti, N.F., Locke, D.H., Phillips, T.H., Pavao-Zuckerman, M., 2024. Interactions between management context and tree water use influence stormwater management potential of urban forests. *Urban Forestry & Urban Greening 95*, 128321. https://doi.org/10.1016/j.ufug.2024.128321

Pontius, R.G., Shusas, E., McEachern, M., 2004. Detecting important categorical land changes while accounting for persistence. *Agriculture, Ecosystems & Environment* 101 (2–3), 251–268. https://doi.org/10.1016/j.agee.2003.09.008

Pontius, R.G., Millones, M., 2011. Death to Kappa: birth of quantity disagreement and allocation disagreement for accuracy assessment. International *Journal of Remote Sensing* 32(15), 4407–4429. https://doi.org/10.1080/01431161.2011.552923

Pontius, R.G., Santacruz, A., 2014. Quantity, exchange, and shift components of difference in a square contingency table. *International Journal of Remote Sensing 35*(21), 7543–7554. https://doi.org/10.1080/2150704x.2014.969814

Pradana, A.N., Djuraidah, A., Soleh, A.M., 2023. Land use change modelling using logistic regression, random forest and additive logistic regression in Kubu Raya Regency, West Kalimantan. *Forum Geografi 37*(2). https://doi.org/10.23917/forgeo.v37i2.23270

Programa de las Naciones Unidas para el Medio Ambiente (PNUMA). Municipio de Loja & Naturaleza y Cultura Internacional, 2007. *Perspectivas del medio ambiente urbano: GEO Loja*. https://wedocs.unep.org/20.500.11822/9269

Sakieh, Y., Jabbarian Amiri, B., Danekar, A., Feghhi, J., Dezhkam, S., 2015. Simulating urban expansion and scenario prediction using a cellular automata urban growth model, SLEUTH, through a case study of Karaj City, Iran. *Journal of Housing and the Built Environment 30*(4), 591–611. https://doi.org/10.1007/s10901-014-9432-2

Samat, N., Hasni, R., Elhadary, Y. a. E., 2011. Modelling Land Use Changes at the Peri-Urban Areas using Geographic Information Systems and Cellular Automata Model. *Journal of Sustainable Development 4*(6). https://doi.org/10.5539/jsd.v4n6p72

Sankarrao, L., Ghose, D.K., Rathinsamy, M., 2021. Predicting land-use change: Intercomparison of different hybrid machine learning models. *Environmental Modelling & Software 145*, 105207. https://doi.org/10.1016/j.envsoft.2021.105207

Sarkar, P., 2000. A brief history of cellular automata. *ACM Computing Surveys 32* (1), 80–107. https://doi.org/10.1145/349194.349202

Schuster-Olbrich, J.P., Marquet, O., Miralles-Guasch, C., Fuentes Arce, L., 2024. Spatial patterns and drivers of urban expansion: An exploratory spatial analysis of the Metropolitan Region of Santiago, Chile, from 1997 to 2013. *Cities 153*, 105305. https://doi.org/10.1016/j.cities.2024.105305

Secretaría de Gestión de Riesgos (SNGR), 2024. *SitRep No. 77 – Incendios forestales (01/01/2024 al 21/11/2024)*. Secretaría de Gestión de Riesgos. https://www.gestionderiesgos.gob.ec/wp-content/uploads/2024/11/SitRep-No.-77-Incendios-Forestales-01012024-al-21112024.pdf

Secretaría de Gestión de Riesgos (SNGR), 2025. *Gobierno nacional declara en emergencia la provincia de Loja*. Secretaría de Gestión de Riesgos. https://www.gestionderiesgos.gob.ec/gobierno-nacional-declara-en-emergencia-la-provincia-de-loja/

Silva, L.P.E., Xavier, A.P.C., Da Silva, R.M., Santos, C.A.G., 2019. Modeling land cover change based on an artificial neural network for a semiarid river basin in northeastern Brazil. *Global Ecology and Conservation 21*, e00811. https://doi.org/10.1016/j.gecco.2019.e00811

Souza, C.M., Shimbo, J.Z., Rosa, M.R., Parente, L.L., Alencar, A.A., Rudorff, B.F.T., Hasenack, H., Matsumoto, M., Ferreira, L.G., Souza-Filho, P.W.M., De Oliveira, S.W., Rocha, W.F., Fonseca, A.V., Marques, C. B., Diniz, C.G., Costa, D., Monteiro, D., Rosa, E.R., Vélez-Martin, E.,… Azevedo, T., 2020. Reconstructing Three Decades of Land Use and Land Cover Changes in Brazilian Biomes with Landsat Archive and Earth Engine. *Remote Sensing 12*(17), 2735. https://doi.org/10.3390/rs12172735

Subedi, P., Subedi, K., Thapa, B., 2013. Application of a hybrid cellular automaton–Markov (CA–Markov) model in land-use change prediction: A case study of Saddle Creek Drainage Basin, Florida. *Journal of Geographic Information System 5*(4), 273–284. https://doi.org/10.4236/jgis.2013.54026

Tahir, Z., Haseeb, M., Mahmood, S.A., Batool, S., Abdullah-Al-Wadud, M., Ullah, S., Tariq, A., 2025. Predicting land use and land cover changes for sustainable land management using CA-Markov modelling and GIS techniques. *Scientific Reports 15*(1). https://doi.org/10.1038/s41598-025-87796-w

Thomas, M., Prakash, A., Dhyani, S., Pujari, P.R., 2024. Governing green change to improve resilience by assessing urban risks for localizing nature-based solutions in fast sprawling Dehradun, India. *International Journal of Disaster Risk Reduction: IJDRR* 111(104684), 104684. https://doi.org/10.1016/j.ijdrr.2024.104684

United Nations Environment Programme (UNEP), Municipality of Loja, Nature and Culture International (NCI). 2007. *Perspectivas del Medio Ambiente Urbano: GEO Loja*. https://wedocs.unep.org/20.500.11822/9269

Van Berkum, S., 2023. How Urban Growth in the Global South Affects Agricultural Dynamics and Food Systems Outcomes in Rural Areas: A Review and Research Agenda. *Sustainability 15*(3), 2591. https://doi.org/10.3390/su15032591

Varnier, M., Weber, E.J., 2025. Evaluating the Accuracy of Land-Use Change Models for Predicting Vegetation Loss Across Brazilian Biomes. *Land 14*(3), 560.

Veldkamp, A., Lambin, E., 2001. Predicting land-use change. *Agriculture Ecosystems & Environment* 85(1–3), 1–6. https://doi.org/10.1016/s0167-8809(01)00199-2

Wu, S., Sumari, N.S., Dong, T., Xu, G., Liu, Y., 2021. Characterizing Urban Expansion Combining Concentric-Ring and Grid-Based Analysis for Latin American Cities. *Land* 10, 444. https://doi.org/10.3390/land10050444

Zhang, M., Zhang, C., Kafy, A.A., Tan, S., 2021. Simulating the relationship between land use/cover change and urban thermal environment using machine learning algorithms in Wuhan City, China. *Land* 11(1), 14.

Zhu, W., Li, Y., Luan, K., Qiu, Z., He, N., Zhu, X., Zou, Z. 2024. Forest Canopy Height Retrieval and Analysis Using Random Forest Model with Multi-Source Remote Sensing Integration. *Sustainability*, 16(5), 1735. https://doi.org/10.3390/su16051735

Supplementary material

A. Reclassification codes for land-cover and land-use categories

ID	Collection 2.0 – MapBiomas Ecuador	Reclassification
1	1. Natural forest	1. Forest
3	1.1. Forest formation	
4	1.2. Open forest	
5	1.3. Mangrove	
6	1.4. Flooded forest	
10	2. Non-forest natural formation	4. Other natural vegetation
11	2.1. Flooded non-forest natural formation	
12	2.2. Grassland or herbaceous formation	
29	2.3. Rocky outcrop	
13	2.4. Other non-forest natural formation	
14	3. Agriculture and forestry	3. Agricultural land
9	3.3. Forestry	
21	3.5. Mosaic of agriculture and/or pasture	
22	4. Non-vegetated area	5. Anthropic
23	4.1. Beach, dune, or sand bank	
24	4.2. Urban infrastructure	
30	4.3. Mining	
68	4.4. Other natural non-vegetated area	
25	4.5. Other anthropic non-vegetated area	
26	5. Water body	2. Water
33	5.1. River, lake, or ocean	
34	5.2. Glacier	
31	5.3. Aquaculture	

B. Transition Probability Matrices for 2070 Scenarios

Trend scenario (with ACMUS and non-urbanizable restrictions)

	Forest	**Water**	**Agricultural land**	**Other natural vegetation**	**Anthropic**
Forest	0.9251	0.0000	0.0448	0.0299	0.0002
Water	0.0102	0.3469	0.1531	0.3878	0.1020
Agricultural land	0.0552	0.0001	0.8631	0.0598	0.0218
Other natural vegetation	0.0896	0.0001	0.1728	0.7280	0.0095
Anthropic	0.0017	0.0000	0.0850	0.0229	0.8905

Intermediate growth scenario (with restrictions)

	Forest	**Water**	**Agricultural land**	**Other natural vegetation**	**Anthropic**
Forest	0.9251	0.0000	0.0448	0.0299	0.0002
Water	0.0102	0.3469	0.1531	0.3878	0.1020
Agricultural land	0.0552	0.0001	0.8631	0.0598	0.0218
Other natural vegetation	0.0896	0.0001	0.1728	0.7280	0.0095
Anthropic	0.0017	0.0000	0.0850	0.0229	0.8905

Accelerated growth scenario (without restrictions)

	Forest	**Water**	**Agricultural land**	**Other natural vegetation**	**Anthropic**
Forest	0.8551	0.0000	0.0648	0.0299	0.0502
Water	0.0102	0.2469	0.1931	0.3878	0.1620
Agricultural land	0.0552	0.0001	0.7631	0.0798	0.1018
Other natural vegetation	0.0896	0.0001	0.2028	0.6280	0.0795
Anthropic	0.0017	0.0000	0.1300	0.0279	0.8404

C. Transition matrices

Transition matrix 1990 – 2000

	A	B	C	D	E	F	G	H	I	J	K
Forest	13,398.35	0.45	630.97	333.56	5.98	14,369.30	329.64	1,300.58	970.95	1,941.90	2,271.53
Water	7.76	3.48	3.39	14.18	1.16	29.97	−21.14	5.35	26.49	10.70	31.84
Agricultural land	984.79	4.28	18,905.15	926.73	268.72	21,089.67	106.59	2,291.12	2,184.53	4,369.05	4,475.64
Other natural vegetation	286.63	0.27	1,573.72	4,287.60	28.18	6,176.40	−491.97	1,396.84	1,888.80	2,793.67	3,285.64
Anthropic	21.40	0.36	83.03	122.36	894.72	1,121.88	76.88	304.04	227.16	454.32	531.19
Total 2000	14,698.94	8.83	21,196.26	5,684.44	1,198.75						

A= Forest; B= Water; C= Agricultural; D= Other natural vegetation; E= Anthropic; F= Total 1990; G= Net change; H= Gains; I= Losses; J= Swap; K= Total change

Transition matrix 2000 – 2010

	A	B	C	D	E	F	G	H	I	J	K
Forest	13,595.62	0.00	660.52	440.31	2.50	14,698.94	576.27	1,679.58	1,103.32	2,206.63	2,782.90
Water	0.09	3.12	1.34	3.39	0.89	8.83	−3.75	1.96	5.71	3.92	7.67
Agricultural land	1,168.03	1.61	18,299.37	1,266.17	461.09	21,196.26	−1,148.50	1,748.39	2,896.89	3,496.78	4,645.28
Other natural vegetation	509.50	0.36	983.62	4,136.65	54.31	5,684.44	190.08	1,737.87	1,547.79	3,095.58	3,285.66
Anthropic	1.96	0.00	102.92	28.00	1,065.86	1,198.75	385.91	518.80	132.89	265.78	651.68
Total 2010	15,275.21	5.08	20,047.76	5,874.51	1,584.66						

A= Forest; B= Water; C= Agricultural; D= Other natural vegetation; E= Anthropic; F= Total 2000; G= Net change; H= Gains; I= Losses; J= Swap; K= Total change

Transition matrix 2010 - 2020

	A	B	C	D	E	F	G	H	I	J	K
Forest	14,587.69	0.00	517.71	168.20	1.61	15,275.21	424.51	1,112.02	687.51	1,375.03	1,799.54
Water	0.00	1.96	2.85	0.27	0.00	5.08	−2.59	0.54	3.12	1.07	3.66
Agricultural land	630.44	0.09	18,615.74	543.57	257.93	20,047.76	341.43	1,773.45	1,432.02	2,864.05	3,205.48
Other natural vegetation	480.25	0.45	1,204.99	4,159.39	29.43	5,874.51	−969.02	746.11	1,715.12	1,492.21	2,461.23
Anthropic	1.34	0.00	47.89	34.07	1,501.36	1,584.66	205.66	288.96	83.30	166.60	372.26
Total 2020	15,699.72	2.50	20,389.19	4,905.50	1,790.32						

A= Forest; B= Water; C= Agricultural; D= Other natural vegetation; E= Anthropic; F= Total 2010; G= Net change; H= Gains; I= Losses; J= Swap; K= Total change

D. Land Use Change Intensity Analysis

Interval level (St) y U

Interval	A	C	St (%/year)
1990–2000	42,787.22	5,297.92	1.238
2000–2010	42,787.23	5,686.61	1.329
2010–2020	42,787.23	3,921.09	0.916

Uniform line (U) = 1.161 %/year

Category level: Gtj (gains)

Interval	Category	Gtj	gains	area_Yt1
1990–2000	Forest	0.885	1,300.58	14,698.93
1990–2000	Water	6.063	5.36	8.84
1990–2000	Agricultural land	1.081	2,291.11	21,196.26
1990–2000	Other natural vegetation	2.457	1,396.83	5,684.43
1990–2000	Anthropic	2.536	304.04	1,198.76
2000–2010	Forest	1.100	1,679.58	15,275.20
2000–2010	Water	3.870	1.97	5.09
2000–2010	Agricultural land	0.872	1,748.40	20,047.77
2000–2010	Other natural vegetation	2.958	1,737.87	5,874.52
2000–2010	Anthropic	3.274	518.79	1,584.65
2010–2020	Forest	0.708	1,112.03	15,699.72
2010–2020	Water	2.160	0.54	2.50
2010–2020	Agricultural land	0.870	1,773.44	20,389.18
2010–2020	Other natural vegetation	1.521	746.11	4,905.50
2010–2020	Anthropic	1.614	288.97	1,790.33

Category level: Lti (losses)

Interval	Category	Lti	loss	area_Yt
1990–2000	Forest	0.676	970.96	14,369.31
1990–2000	Water	8.839	26.49	29.97
1990–2000	Agricultural land	1.036	2,184.52	21,089.67
1990–2000	Other natural vegetation	3.058	1,888.80	6,176.40
1990–2000	Anthropic	2.025	227.15	1,121.87
2000–2010	Forest	0.751	1,103.33	14,698.95
2000–2010	Water	6.467	5.71	8.83
2000–2010	Agricultural land	1.367	2,896.90	21,196.27
2000–2010	Other natural vegetation	2.723	1,547.79	5,684.44
2000–2010	Anthropic	1.108	132.88	1,198.74
2010–2020	Forest	0.450	687.52	15,275.21
2010–2020	Water	6.142	3.12	5.08
2010–2020	Agricultural land	0.714	1,432.03	20,047.77
2010–2020	Other natural vegetation	2.920	1,715.12	5,874.51
2010–2020	Anthropic	0.526	83.30	1,584.66

Transition level: R_tin and W_tn

Interval	Category from	Category to	R_tin	W_tn	Transition area	area_i_Yt	gains_n	non_n_ area_Yt
1990–2000	Water	Forest	2.589	0.458	7.76	29.97	1,300.58	28,417.91
1990–2000	Agricultural land	Forest	0.467	0.458	984.79	21,089.67	1,300.58	28,417.91
1990–2000	Other natural vegetation	Forest	0.464	0.458	286.63	6,176.40	1,300.58	28,417.91
1990–2000	Antrópico	Forest	0.191	0.458	21.40	1,121.87	1,300.58	28,417.91
1990–2000	Forest	Water	0.000	0.001	0.45	14,369.31	5.36	42,757.25
1990–2000	Agricultural land	Water	0.002	0.001	4.28	21,089.67	5.36	42,757.25
1990–2000	Other natural vegetation	Water	0.000	0.001	0.27	6,176.40	5.36	42,757.25
1990–2000	Antrópico	Water	0.003	0.001	0.36	1,121.87	5.36	42,757.25
1990–2000	Forest	Agricultural land	0.439	1.056	630.97	14,369.31	2,291.11	21,697.55
1990–2000	Water	Agricultural land	1.131	1.056	3.39	29.97	2,291.11	21,697.55
1990–2000	Other natural vegetation	Agricultural land	2.548	1.056	1,573.72	6,176.40	2,291.11	21,697.55
1990–2000	Antrópico	Agricultural land	0.740	1.056	83.03	1,121.87	2,291.11	21,697.55
1990–2000	Forest	Other natural vegetation	0.232	0.382	333.56	14,369.31	1,396.83	36,610.82
1990–2000	Water	Other natural vegetation	4.731	0.382	14.18	29.97	1,396.83	36,610.82
1990–2000	Agricultural land	Other natural vegetation	0.439	0.382	926.73	21,089.67	1,396.83	36,610.82
1990–2000	Antrópico	Other natural vegetation	1.091	0.382	122.36	1,121.87	1,396.83	36,610.82
1990–2000	Forest	Anthropic	0.004	0.073	5.98	14,369.31	304.04	41,665.35
1990–2000	Water	Anthropic	0.387	0.073	1.16	29.97	304.04	41,665.35
1990–2000	Agricultural land	Anthropic	0.127	0.073	268.72	21,089.67	304.04	41,665.35
1990–2000	Other natural vegetation	Anthropic	0.046	0.073	28.18	6,176.40	304.04	41,665.35
2000–2010	Water	Forest	0.102	0.598	0.09	8.83	1,679.58	28,088.28
2000–2010	Agricultural land	Forest	0.551	0.598	1,168.03	21,196.27	1,679.58	28,088.28
2000–2010	Other natural vegetation	Forest	0.896	0.598	509.50	5,684.44	1,679.58	28,088.28
2000–2010	Anthropic	Forest	0.016	0.598	1.96	1,198.74	1,679.58	28,088.28
2000–2010	Forest	Water	0.000	0.000	0.00	14,698.95	1.97	42,778.40
2000–2010	Agricultural land	Water	0.001	0.000	1.61	21,196.27	1.97	42,778.40
2000–2010	Other natural vegetation	Water	0.001	0.000	0.36	5,684.44	1.97	42,778.40

2000–2010	Anthropic	Water	0.000	0.000	0.00	1,198.74	1.97	42,778.40
2000–2010	Forest	Agricultural land	0.449	0.810	660.52	14,698.95	1,748.40	21,590.96
2000–2010	Water	Agricultural land	1.518	0.810	1.34	8.83	1,748.40	21,590.96
2000–2010	Other natural vegetation	Agricultural land	1.730	0.810	983.62	5,684.44	1,748.40	21,590.96
2000–2010	Anthropic	Agricultural land	0.859	0.810	102.92	1,198.74	1,748.40	21,590.96
2000–2010	Forest	Other natural vegetation	0.300	0.468	440.31	14,698.95	1,737.87	37,102.79
2000–2010	Water	Other natural vegetation	3.839	0.468	3.39	8.83	1,737.87	37,102.79
2000–2010	Agricultural land	Other natural vegetation	0.597	0.468	1,266.17	21,196.27	1,737.87	37,102.79
2000–2010	Anthropic	Other natural vegetation	0.234	0.468	28.00	1,198.74	1,737.87	37,102.79
2000–2010	Forest	Anthropic	0.002	0.125	2.50	14,698.95	518.79	41,588.49
2000–2010	Water	Anthropic	1.008	0.125	0.89	8.83	518.79	41,588.49
2000–2010	Agricultural land	Anthropic	0.218	0.125	461.09	21,196.27	518.79	41,588.49
2000–2010	Other natural vegetation	Anthropic	0.096	0.125	54.31	5,684.44	518.79	41,588.49
2010–2020	Water	Forest	0.000	0.404	0.00	5.08	1,112.03	27,512.02
2010–2020	Agricultural land	Forest	0.314	0.404	630.44	20,047.77	1,112.03	27,512.02
2010–2020	Other natural vegetation	Forest	0.818	0.404	480.25	5,874.51	1,112.03	27,512.02
2010–2020	Anthropic	Forest	0.008	0.404	1.34	1,584.66	1,112.03	27,512.02
2010–2020	Forest	Water	0.000	0.000	0.00	15,275.21	0.54	42,782.15
2010–2020	Agricultural land	Water	0.000	0.000	0.09	20,047.77	0.54	42,782.15
2010–2020	Other natural vegetation	Water	0.001	0.000	0.45	5,874.51	0.54	42,782.15
2010–2020	Anthropic	Water	0.000	0.000	0.00	1,584.66	0.54	42,782.15
2010–2020	Forest	Agricultural land	0.339	0.780	517.71	15,275.21	1,773.44	22,739.46
2010–2020	Water	Agricultural land	5.610	0.780	2.85	5.08	1,773.44	22,739.46
2010–2020	Other natural vegetation	Agricultural land	2.051	0.780	1,204.99	5,874.51	1,773.44	22,739.46
2010–2020	Anthropic	Agricultural land	0.302	0.780	47.89	1,584.66	1,773.44	22,739.46
2010–2020	Forest	Other natural vegetation	0.110	0.202	168.20	15,275.21	746.11	36,912.72
2010–2020	Water	Other natural vegetation	0.531	0.202	0.27	5.08	746.11	36,912.72

2010–2020	Agricultural land	Other natural vegetation	0.271	0.202	543.57	20,047.77	746.11	36,912.72
2010–2020	Anthropic	Other natural vegetation	0.215	0.202	34.07	1,584.66	746.11	36,912.72
2010–2020	Forest	Anthropic	0.001	0.070	1.61	15,275.21	288.97	41,202.57
2010–2020	Water	Anthropic	0.000	0.070	0.00	5.08	288.97	41,202.57
2010–2020	Agricultural land	Anthropic	0.129	0.070	257.93	20,047.77	288.97	41,202.57
2010–2020	Other natural vegetation	Anthropic	0.050	0.070	29.43	5,874.51	288.97	41,202.57